GEORG-AUGUST-UNIVERSITÄT
GÖTTINGEN

Fakultät für
Physik

Bachelor's Thesis

b-Tagging zur Verbesserung der Top-Quark-Rekonstruktion

b-Tagging in Order to Improve the Top Quark Reconstruction

prepared by

Philipp Stolte

from Göttingen

at the II. Institute of Physics

Thesis number:	II.Physik-UniGö-BSc-2010/02
Thesis period:	April 12, 2010 until July 19, 2010
Supervisors:	Dr. Kevin Kröninger Dipl. Phys. Stefan Guindon, BSc.
First Referee:	Prof. Dr. Arnulf Quadt
Second Referee:	Prof. Dr. Ariane Frey

Abstract

b-tagging can be described as the proper identification of jets originating from bottom (b) quarks. In one instance, these quarks are created by the decay of top-antitop quark pairs. In this bachelor's thesis, the impact of several b-tagging methods on the reconstruction of such top-antitop quark pairs in the semileptonic decay channel with four jets, one electron and a neutrino in the final state is analyzed by use of the *Kinematic Likelihood Fitter* (KLFitter), a tool for kinematic fitting based on a likelihood approach.
After testing the initial version of the KLFitter, two different b-tagging algorithms are examined with this program, both depending on the calculation of jet weights. The additional b-tagging information improves the b-tagging efficiency and, in this context, the reconstruction efficiency of the KLFitter as well. The latter is essential for a more precise measurement of the top quark properties based on an adequate reconstruction of the decay of this heaviest quark. Subsequently, the total efficiency of the fitter, combining the reconstruction and a so-called matching efficiency, can be estimated.
With the improvements of the KLFitter, established in the framework of this thesis, it has become an even more promising tool for analyzing top quark decays being detected at the *Large Hadron Collider* (LHC) in the near future, thus helping to determine the properties of the top quark, for example, its mass.

Zusammenfassung

b-Tagging kann als das korrekte Identifizieren von aus b-Quarks hervorgehenden Jets verstanden werden. Diese Quarks entstehen zum Beispiel beim Zerfall von Top-Antitop-Quark-Paaren. In dieser Bachelorarbeit soll der Einfluss verschiedener Methoden des b-Taggings auf die Rekonstruktion solcher Top-Antitop-Quark-Paare im semileptonischen Zerfallskanal mit vier Jets, einem Elektron und einem Neutrino im Endzustand untersucht werden. Dabei findet der *Kinematic Likelikood Fitter* (KLFitter) Verwendung, ein Werkzeug, welches zum kinematischen Fitten unter Ausnutzung einer Likelihood-Methode dient.
Nach einigen Tests mit der ursprünglichen Version des KLFitters sollen mit diesem Programm zwei verschiedene b-Tagging-Verfahren, die beide auf der Berechnung von Jetgewichten beruhen, untersucht werden. Die dem KLFitter hinzugefügten Informationen bezüglich des b-Taggings bewirken eine Erhöhung der Effizienz jenes Taggings und folglich eine Erhöhung der Rekonstruktionseffizienz. Letzteres ist für eine genauere Messung der Eigenschaften des Top Quarks bedeutsam, da eine solche auf der möglichst präzisen Rekonstruktion des Top-Quark-Zerfalls fußt. Schließlich kann die Gesamteffizienz des Fitters abgeschätzt werden, die sich aus der Kombination der Rekonstruktions- und einer sogenannten Abgleichseffizienz ergibt.
Mit den im Rahmen dieser Bachelorarbeit entwickelten Verbesserungen wurde der KLFitter hin zu einem vielversprechenden Werkzeug entwickelt, welches in naher

Zukunft zur Analyse von Top-Quark-Zerfällen am *Large Hadron Collider* (LHC) herangezogen werden kann und somit bei der Bestimmung von Eigenschaften des Top-Quarks, wie zum Beispiel dessen Masse, behilflich sein wird.

Contents

1 Introduction

"What is matter made of?" This question has bothered physicists for centuries. Elementary particle physics addresses it at the smallest scales. In recent decades, many elementary particles were discovered, which we can now regard as the first steps helping to find an answer to the central question mentioned at the beginning. Today's experiments in the field of elementary particle physics are based on collisions of particles getting their high energy from accelerators. That is why the expression *High Energy Physics* is also commonly used in order to describe such particle accelerator experiments. The detection of the decay products originating from the collisions of such heavily accelerated particles is essential to draw conclusions about these processes and the properties of the involved particles.
The smaller the scale of observed processes, the higher energies and, as a consequence thereof, larger colliders are necessary to improve our knowledge of elementary particles. Today, the *Large Hadron Collider* (LHC) at CERN is the most powerful particle accelerator. The LHC is designed to reach beam energies of more than 7 TeV associated with the hope that this energy is sufficient to find the Higgs particle which has not been detected so far as well as to test the *Standard Model of Elementary Particle Physics* (SM). Furthermore, the new energy region may include possible supersymmetric particles or something completely unexpected which can be described as physics beyond the SM.

The LHC serves to produce, among other particles, top quarks. This quark is a field of strong interest due to its very short lifetime of about 10^{-25} s and its huge mass which is of the order of the gold atom mass. The properties of the top quark are of special interest because, for example, the measurements of the top quark mass help to limit the prediction of the Higgs boson mass. Moreover, this heaviest quark could also provide a sign of new physics beyond the SM.
The top mass can be measured more precisely by the reconstruction of detected top quark decays. $t\bar{t}$ events, where the top (t) and its antiparticle ($\bar{t}$) decay, are

more frequently produced than single top quarks. As the top quark decays into a bottom quark and a W boson in most cases, there are at least two jets originating from b quarks in the detector. But since the W boson is not stable, its decay can lead to further jets in the detector, which complicates the identification of both b jets. However, an identification of b jets is an essential part of reconstructing the top quark decay, which is, in turn, relevant for calculating the top quark properties with a high precision. Thus, the identification or *tagging* of b quarks plays an important role to identify top quarks. An improvement of the b-tagging efficiency can be described as a very useful means for a better reconstruction of top-antitop pairs and the calculation of the top mass, respectively.
In this thesis, different methods of implementing b-tagging in the *Kinematic Likelihood Fitter* are presented. The *KLFitter* is a program which can be described as a library for kinematic fitting using a likelihood approach in order to reconstruct top-antitop pair decays. The studies performed in this thesis will be significant for the reconstruction of top quark decays being detected by the ATLAS experiment at the LHC.

The following chapter can be regarded as an introductory review presenting some fundamental aspects of the Standard Model of Particle Physics. Special emphasis is placed on the top quark and its properties. The just mentioned facts and information about the top quark decay are explained in more detail. In the subsequent Chapter 3, the ATLAS detector constructed at the LHC is briefly presented. A short introduction into the fundamentals of b-tagging is given in the fourth Chapter whereas Chapter 5 contains a more detailed description of the KLFitter as well as some information concerning the sample, consisting of events generated by Monte Carlo simulations, which is used for testing the top reconstruction efficiency of the Kinematic Likelihood Fitter. In Chapter 6, the studies done in order to improve the b-tagging efficiency and the reconstruction efficiency, respectively, by testing various b-tagging methods are presented. Finally, a short summary of the most important results can be found in Chapter 7.

2 The Standard Model and the Importance of the Top Quark Therein

As the main subject of this thesis is the reconstruction of top quark decays, this chapter presents the most important theoretical background concerning the top quark and its properties as well as the production and the decay of top quarks with emphasis on the decay of top-antitop pairs. To begin, a short summary of fundamental aspects of the Standard Model of Particle Physics is depicted.

2.1 The Standard Model of Particle Physics

The *Standard Model of Particle Physics* (SM) is a theory emerging from the 1960s and 1970s which describes all of the known elementary particle interactions, except gravity. The theory is based on two families of elementary particles, quarks and leptons, and incorporates quantum electrodynamics, the Glashow-Weinberg-Salam theory of electroweak processes as well as quantum chromodynamics. The interactions between all quarks and leptons, which are initially massless and whose mass is generated by the so-called Higgs mechanism (according to electroweak theory), are mediated by gauge bosons. The Higgs boson is a massive scalar elementary particle predicted by the SM. However, it has not been observed up to now [1].
The SM has met every experimental test since the mid-20th century. Nevertheless, it does not include, for example, gravitation or dark matter as well as nonzero neutrino masses although these are described by extensions.

2.1.1 Quarks, Leptons and Mediators

All matter is made of three kinds of elementary particles: leptons, quarks and mediators. Both quarks and leptons are also called *fermions* as they are spin-$\frac{1}{2}$-particles. The mediators or so-called gauge *bosons* carry integer spin.
There are six leptons classified by charge Q, electron number L_e, muon number L_μ and tau number L_τ. Similarly, there are six "flavours" of quarks, classified by charge, upness U, downness D, strangeness S, charm C, bottomness B and topness T. Leptons and quarks fall naturally into three *generations*, each. The same applies to antifermions [2].
As two quarks or leptons belong to one generation forming a doublet, all three lepton generations can be written as follows:

$$\begin{pmatrix} \nu_e \\ e \end{pmatrix}, \qquad \begin{pmatrix} \nu_\mu \\ \mu \end{pmatrix}, \qquad \begin{pmatrix} \nu_\tau \\ \tau \end{pmatrix}.$$

Each lepton generation consists of an electrically neutral neutrino ν_i and a lepton with charge $Q = e$. The three up-type quarks (u, c, t) with charge $Q = \frac{2}{3}e$ and down-type quarks (d, s, b) with charge $Q = -\frac{1}{3}e$ are arranged into generations according to the following diagram:

$$\begin{pmatrix} u \\ d \end{pmatrix}, \qquad \begin{pmatrix} c \\ s \end{pmatrix}, \qquad \begin{pmatrix} t \\ b \end{pmatrix}.$$

However, writing quarks and leptons just as doublets is an oversimplification since chirality or handedness is not taken into account. All fermions which have been considered so far form left-handed *doublets* but right-handed *singlets*. The theory of electroweak interaction demands a new quantum number, the *weak isospin*, which is different for left-handed and right-handed particles. In the following Table 2.1, all particles are listed. It includes particle properties such as spin s, the third component T_3 of weak isospin T, electric charge Q and colour C. The *weak hypercharge* Y_W which is calculated according to $Y_W = 2(Q - T_3)$ is also added [2, 3].

It is important to mention that Table 2.1 contains the weak eigenstates d', s' and b' which are different from the mass eigenstates representing the "physical" quarks d, s and b. The weak eigenstates are linear combinations of the mass eigenstates and the coefficients can be written in a matrix, the Cabibbo matrix with the Cabibbo angle, if only the mixing of the first two quark generations is considered. Kobayashi and

Particles				Q $[e]$	C	s	T_3	Y_W
Leptons	$\begin{pmatrix}\nu_e\\ e\end{pmatrix}_L$	$\begin{pmatrix}\nu_\mu\\ \mu\end{pmatrix}_L$	$\begin{pmatrix}\nu_\tau\\ \tau\end{pmatrix}_L$	$\begin{pmatrix}0\\ -1\end{pmatrix}$	-	$\frac{1}{2}$	$\begin{pmatrix}+\frac{1}{2}\\ -\frac{1}{2}\end{pmatrix}$	-1
	e_R	μ_R	τ_R	-1	-	$\frac{1}{2}$	0	-2
Quarks	$\begin{pmatrix}u\\ d'\end{pmatrix}_L$	$\begin{pmatrix}c\\ s'\end{pmatrix}_L$	$\begin{pmatrix}t\\ b'\end{pmatrix}_L$	$\begin{pmatrix}+\frac{2}{3}\\ -\frac{1}{3}\end{pmatrix}$	r,g,b	$\frac{1}{2}$	$\begin{pmatrix}+\frac{1}{2}\\ -\frac{1}{2}\end{pmatrix}$	$+\frac{1}{3}$
	u_R	c_R	t_R	$+\frac{2}{3}$	r,g,b	$\frac{1}{2}$	0	$+\frac{4}{3}$
	d_R	s_R	b_R	$-\frac{1}{3}$	r,g,b	$\frac{1}{2}$	0	$-\frac{2}{3}$
Gauge Bosons	Photon γ			0	-	1	0	0
	Z^0			0	-	1	0	0
	$W^\pm$			± 1	-	1	± 1	0
	8 Gluons g			0	r,g,b	1	0	0

Table 2.1: Particles and mediators in the Standard Model. The particle properties electric charge Q, colour C, spin s, the third component T_3 of weak isospin T as well as weak hypercharge Y_W are listed [2, 3].

Maskawa generalized the Cabibbo scheme to handle all three quark generations. The weak eigenstates are related to the physical quark states by the so-called *CKM matrix* V [2]:

$$\begin{pmatrix} d' \\ s' \\ b' \end{pmatrix} = \begin{pmatrix} V_{ud} & V_{us} & V_{ub} \\ V_{cd} & V_{cs} & V_{cb} \\ V_{td} & V_{ts} & V_{tb} \end{pmatrix} \cdot \begin{pmatrix} d \\ s \\ b \end{pmatrix}.$$

This unitary matrix V has three real parameters and one imaginary one, a phase factor, causing CP (*charge parity*) violation. To discuss CP violation, the Wolfenstein parametrization of the CKM matrix is used [4].

As the top quark reconstruction helps to measure the top mass more accurately, the masses of all leptons and quarks are listed in the following table, making it obvious how large the top mass is, in comparison to the mass of all other elementary particles. This fact underlines the special importance of the top quark in the SM. As Table 2.2 reveals, the considered fermion masses are spread over a large range. Incidentally, antifermions have the same mass as the corresponding fermions as long as CPT (*charge parity time*) is conserved.

Lepton	Mass m in [MeV]	Quark	Mass m in [MeV]
e	0.510998910 ± 13	u	$2.55^{+0.75}_{-1.05}$
μ	105.6583668 ± 38	c	1270^{+70}_{-110}
τ	1776.84 ± 0.17	t	$173100 \pm 600 \pm 1100$
ν_e	$< 2 \cdot 10^{-6}$	d	$5.04^{+0.96}_{-1.54}$
ν_μ	$< 2 \cdot 10^{-6}$	s	105^{+25}_{-35}
ν_τ	$< 2 \cdot 10^{-6}$	b	4200^{+170}_{-70}

Table 2.2: Masses of fermions [1].

2.1.2 Interactions

The Standard Model incorporates three elementary particle interactions including electromagnetic, weak and strong interactions. As the SM is a gauge theory, these interactions can be expressed by *local gauge symmetries*. As a consequence, the *Lagrangian* is locally invariant under a transformation of a certain gauge group, which is also a *Lie group*. Local gauge symmetries can be described by unitary and special unitary Lie groups (U and SU). The number of gauge fields associated with a certain interaction, which is equal to the number of generators of a group, is n^2 ($U(n)$ group) or n^2-1 ($SU(n)$ group), respectively. The number n^2-1 corresponds to the dimension of a group which has order n.
The Lie group $U(1)_{\text{em}}$ is used to describe electromagnetic interactions. The underlying phase transformation is $\phi \rightarrow \phi' = \mathrm{e}^{\mathrm{i}\theta}\phi$ with spinor field ϕ and a real number θ. Weak interactions are mathematically expressed by a $SU(2)$ group, which is generated by the three *Pauli matrices* σ_i with $i = 1, 2, 3$. Thus, the phase transformation is $\phi \rightarrow \phi' = \mathrm{e}^{\mathrm{i}\vec{\sigma}\vec{a}}\phi$ with $\vec{a} = (a_1, a_2, a_3)$ and $a_1, a_2, a_3 \in \mathbb{R}$. In electroweak theory, both weak and electromagnetic interactions are unified to the symmetry group $SU(2)_L \otimes U(1)_Y$. The index L indicates that the weak isospin current couples only to left-handed fermions. Y signifies the weak hypercharge, previously denoted as Y_W. In this way, $U(1)_{\text{em}}$ is a subgroup of this group [5].
The group $SU(2)_L \otimes U(1)_Y$ consists of an isotriplet of vector fields W^i_μ (gauge fields of $SU(2)_L$) with a coupling strength called g and a weak isospin current J^i_μ as well as a single vector field B_μ (gauge field of $U(1)_Y$) coupled to the weak hypercharge current j^Y_μ whose strength is conventionally defined as $\frac{g'}{2}$. Then, the basic electroweak interaction results in:

$$-\mathrm{i}g(J^i)^\mu W^i_\mu - \mathrm{i}\frac{g'}{2}(j^Y)^\mu B_\mu.$$

The fields $W_\mu^\pm$ are used to characterize massive charged bosons ($W^\pm$) whereas W_μ^3 and B_μ represent neutral fields. Both neutral fields mix in a way that the mass eigenstates can be written as:

$$\begin{aligned} A_\mu &= B_\mu \cos\theta_W + W_\mu^3 \sin\theta_W \qquad \text{(massless boson } \gamma\text{)}, \\ Z_\mu &= -B_\mu \sin\theta_W + W_\mu^3 \cos\theta_W \qquad \text{(massive boson } Z^0\text{)}. \end{aligned}$$

θ_W is the so-called Weinberg angle with $\sin^2\theta_W \approx 0.23$. Together with

$$W_\mu^\pm = \sqrt{\frac{1}{2}}(W_\mu^1 \mp \mathrm{i}W_\mu^2) \qquad \text{(massive charged bosons } W^\pm\text{)},$$

all electroweak gauge bosons are described. Massive gauge bosons lead to a symmetry breaking of the $SU(2)_L \otimes U(1)_Y$ group. To generate the particle masses in a gauge invariant way, the Higgs mechanism with the so-called Higgs boson needs to be introduced [6].
Quantum chromodynamics is described by the symmetry group $SU(3)_C$, generated by the eight *Gell-Mann matrices* λ_k, $k = 1, ..., 8$. As the gluon is the associated gauge boson, there are eight gluon fields $G_{\mu\nu}^k$ carrying colour charge (red, blue, green), which is denoted by the index C, themselves. Finally, the electroweak as well as the strong interactions can be put together to form the *Standard Model Symmetry Group*:

$$SU(3)_C \otimes SU(2)_L \otimes U(1)_Y.$$

Electromagnetic interactions are mediated by photons whereas strong interactions are mediated by gluons. W and Z bosons belong to weak interactions. The mediators and their properties are listed in Table 2.3. The theory behind these interactions is mentioned as well. In contrast to the other fundamental forces, the strong force increases with distance. This effect is known as *quark confinement* and explains why free quarks cannot be observed [2, 5].

Although SM predictions could be tested very successfully in recent years, the Standard Model is not seen as a complete theory as neither the physics of general relativity such as gravitation, nor dark energy is incorporated. Other problems include matter-anitimatter-imbalance which has yet to be added to the SM framework.

Force	Rel. strength	Theory	Mediator	Mass in [GeV]
Strong	10	Chromodynamics	Gluon	0
EM	10^{-2}	Electrodynamics	Photon	0
Weak	10^{-13}	Flavordynamics	W	80.398 ± 0.025
			Z	91.1876 ± 0.0021

Table 2.3: The three fundamental forces explained by the Standard Model and their properties [1, 2]. Since "relative strength" is an ambiguous notion, several sources offer different figures. "EM" means "electromagnetic".

2.2 The Top Quark

The idea of having three quark generations appeared in 1973, when KOBAYASHI and MASKAWA postulated the 3×3 CKM matrix as a generalization of the Cabibbo matrix. Due to its properties, as given in the following subsection, the top quark as a third generation quark was first detected in $t\bar{t}$ production in 1995, a long time after its prediction. The heaviest of all six quarks was discovered by the CDF and DØ experiments in $p\bar{p}$ collisions at Tevatron Run I at $\sqrt{s} = 1.8$ TeV [7, 8]. A few years later, in 2009, both collaborations confirmed the discovery of electroweak single top quark production at Tevatron Run II at $\sqrt{s} = 1.96$ TeV [9, 10]. Because of its comparatively huge mass, the top quark could be related to electroweak symmetry breaking mechanisms. In this context, this quark would also be able provide a sign of physics beyond the SM, making it essential to measure its properties. Some of those are mentioned in the next subsection. Production mechanisms and decay schemes of the top quark are also discussed.

2.2.1 Top Quark Properties

Together with its weak isospin partner, the bottom quark, the top quark forms the third quark generation. It is assumed to carry charge $Q = +\frac{2}{3}e$ and spin $s = \frac{1}{2}$ although these properties have not yet been measured.

The top quark mass determinations realized in the last few years are based on $p\bar{p}$ collisions at the Tevatron. The current world average is an average of top mass measurements from Tevatron Run I and Run II from both Tevatron experiments

CDF and DØ. It uses correlated uncertainties to produce a better estimate [11]:

$$m_t = 173.3 \pm 0.6 \pm 0.9 \ \frac{\text{GeV}}{c^2}.$$

The total uncertainty can be calculated to $\sigma_{\text{tot}} = \sqrt{\sigma_{\text{stat}}^2 + \sigma_{\text{syst}}^2} \approx 1.25 \ \frac{\text{GeV}}{c^2}$. A comparison between this value and the top mass reveals a high relative precision of the top mass measurement which outvalues the precision of all other measured quark masses: $\sigma_{\text{rel}} = \frac{\sigma_{\text{tot}}}{m_t} \approx 0.72\%$.

The top quark predominantly decays via $t \to Wq$, where $q = d, s, b$. According to the CKM matrix, it is $V_{tb} \approx 1$ and thus the heaviest quark decays to almost 100% into Wb. This results in an extremely short lifetime of about [12]:

$$\tau_t = \frac{1}{\Gamma_t} \approx 5 \cdot 10^{-25}.$$

As it takes about $\tau_{\text{had}} \approx 3 \cdot 10^{-24}$ s to form hadrons, the top quark decays before hadronisation occurs. That is why toponium states, mesons consisting of t and $\bar{t}$, cannot exist. The total width $\Gamma = \frac{\hbar}{\tau}$ is proportional to $|V_{tb}|^2$ and furthermore depends on $\frac{m_W}{m_t}$ with the W boson mass m_W according to Fermi's Golden Rule and [12]:

$$\Gamma(t \to Wb) = \frac{G_F}{8\pi\sqrt{2}} \cdot m_t^3 |V_{tb}|^2 \left(1 - 3\left(\frac{m_W}{m_t}\right)^4 + 2\left(\frac{m_W}{m_t}\right)^6\right).$$

G_F is the Fermi coupling constant. This decay width can be calculated via the Born approximation: $\Gamma_t^B \approx 1.44$ GeV. With the QCD coupling α_s, which depends on m_t, one can calculate the total decay width by using $m_t = 171 \frac{\text{GeV}}{c^2}$ according to [13, 14]:

$$\Gamma(t \to Wb) = \Gamma_t^B \cdot (1 - 0.81\alpha_s - 1.81\alpha_s^2) \approx 1.28 \text{ GeV}.$$

2.2.2 Top Quark Production

Top quarks are produced either as a single quark or as $t\bar{t}$ pairs.

Top-Antitop Quark Pairs Top-antitop quark pairs $t\bar{t}$ are produced via the strong interaction, or more precisely, via $q\bar{q}$ annihilation or via gg fusion. Perturbative quantum chromodynamics is used to describe top pair production at high energy in-

teractions of $p\bar{p}$ (at the Tevatron) or pp (at the LHC) collisions. Such hard scattering processes result in an interaction between the quarks and gluons as the constituents of both colliding hadrons. Altogether, there are three leading order Feynman diagrams to illustrate gluon fusion $gg \to t\bar{t}$ and there exists one for $q\bar{q} \to t\bar{t}$, which is illustrated in Fig. 2.1.

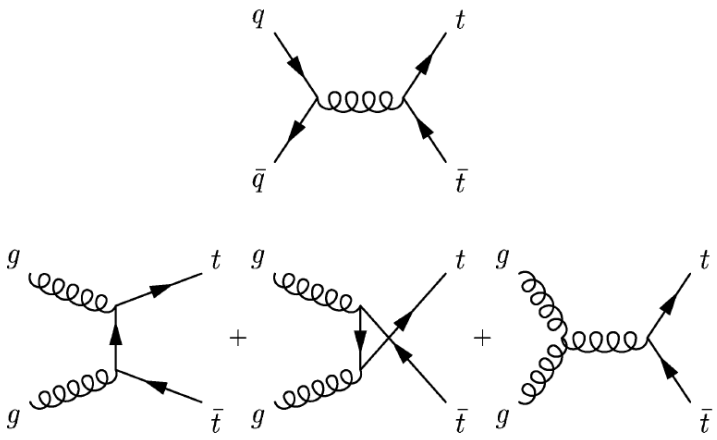

Figure 2.1: Top-antitop quark pair production via the strong interaction - lowest order diagrams of $q\bar{q}$ annihilation (top) and of gluon fusion (bottom).

The center-of-mass energy $\sqrt{s}$ is responsible for the relative contributions of both production possibilities to the total cross section due to the parton density function [15]. The so-called Bjorken-x describes the ratio of a parton momentum to the total momentum. In the case of $t\bar{t}$ production, one can deduce for the minimal x: $x \approx \frac{2m_t}{\sqrt{s}}$ [16]. At small x, the values of the parton densities of the gluons exceed the ones of the quarks. Consequently, the $t\bar{t}$ production is dominated by annihilation of $q\bar{q}$ at the Tevatron. According to the higher center-of-mass energy of the LHC, $t\bar{t}$ pairs are mainly produced via gg fusion there. At Tevatron Run II with $\sqrt{s} = 1.96$ TeV, 85% of all top quark pairs originated from $q\bar{q}$ annihilation, 15% from gluon fusion. At the LHC, when it reaches $\sqrt{s} = 14$ TeV, about 90% of all $t\bar{t}$ pairs will be produced by gluon fusion, 10% by quark-antiquark annihilation [16].

Single Top Quarks Through the weak interaction the production of a single top quark is feasible via the processes in Fig. 2.2 where the production is mediated by a W boson in the s-channel or the t-channel. The total single top production cross section (σ_s belonging to the s-, σ_t to the t-channel) is not considerably smaller than

the $t\bar{t}$ production cross section, but to isolate such an event from backgrounds is more demanding as fewer jets appear. Since σ_s as well as σ_t are proportional to $|V_{tb}|^2$, an experimental measurement of these cross sections provides a direct measurement of the CKM matrix element $|V_{tb}|$ [17]. The single top quark production processes, as mentioned above, were observed at the Tevatron in 2009 [9, 10].

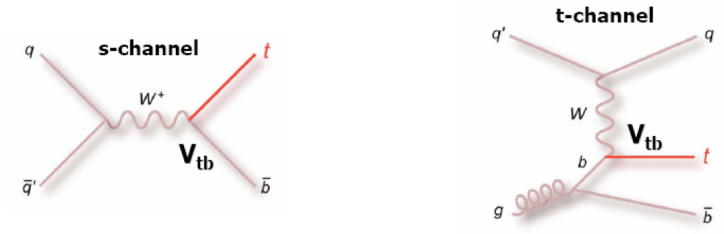

Figure 2.2: Single top quark production processes - s-channel and t-channel.

2.2.3 Top Quark Decays

In this subsection, some information briefly presented in the introduction is now explained in a more detailed way. Unitarity of the CKM matrix as well as the assumption of three quark generations leads to:

$$V_{td}^* V_{dt} + V_{ts}^* V_{st} + V_{tb}^* V_{bt} = |V_{td}|^2 + |V_{ts}|^2 + |V_{tb}|^2 = 1.$$

The analysis of data originating from weak decays of hadrons yields $0.9990 < |V_{tb}| < 0.9992$ at 95% C.L. [1], which is an expected range because of approximate diagonality of the CKM matrix. The branching ratios are calculated to be:

$$\mathcal{B}(t \to bW) = 0.998, \qquad \mathcal{B}(t \to sW) \approx 1.9 \cdot 10^{-3}, \qquad \mathcal{B}(t \to dW) \approx 10^{-4}.$$

Thus, the top quark decays almost exclusively into a b quark and a W^+ boson, its antiparticle into an anti-bottom quark and a W^- boson. Both b quarks of a $t\bar{t}$ decay hadronize to jets. These jets contain B mesons, which may have a decay vertex displaced from the original interaction point, which is the so-called *primary vertex* (see Chapter 4). This fact allows for a distinction between b jets and jets originating from light quarks. The W bosons can decay into two light quarks q_1 and $\overline{q_2}$ which again form jets (hadronic decay) or, alternatively, into a charged lepton and the corresponding antineutrino (leptonic decay). As both W bosons decay entirely

independently and as the order of both decays is not important, the following combinations of the two decay channels are possible: *all-jets*, *dileptonic* or *semileptonic*. The latter implies that one W decays into quarks while the other decays leptonically. In Table 2.4 the branching ratios $\mathcal{B}$ of the independent channels are listed. Multiplying these numbers leads to the branching ratios of the combined $t\bar{t}$ decays. A certain colour factor N_C with $N_C^{\text{lep}} = 1$ and $N_C^{\text{had}} = 3$ has to be considered.

Final states	W	$e\nu_e$	$\mu\nu_\mu$	$\tau\nu_\tau$	$u\bar{d}/d\bar{u}$	$c\bar{s}/s\bar{c}$
N_C		1	1	1	3	3
$\mathcal{B}$		$\frac{1}{9}$	$\frac{1}{9}$	$\frac{1}{9}$	$\frac{1}{3}$	$\frac{1}{3}$

Table 2.4: Branching ratios of the final states from W boson decays. For the hadronic decays, the most probable final state according to the CKM matrix is listed. The products of the hadronic decay depend on the charge of the originating W. Hence, both possibilities are mentioned.

Since final states containing τ mesons are difficult to identify, they are disregarded, which leads to the following probabilities of leptonic and hadronic decay:

$$P(\text{had}) = \frac{2}{3} \qquad \text{and} \qquad P(\text{lep}) = \frac{2}{9}.$$

The three different decay channels can be analyzed in more detail [16–18]:

All-jets Decay Channel Both W bosons decay into quarks. The branching ratio for this decay is $\mathcal{B} = \frac{2}{3} \cdot \frac{2}{3} = \frac{4}{9}$, that is comparatively large. But the six jet signature is similar to that of QCD multijet background. However, this channel has the advantage, that no missing transverse momentum from the neutrino, as in the following two decay channels, has to be taken into account.

Dileptonic Decay Channel In this instance, both bosons decay leptonically in an electron or a muon. Thus $\mathcal{B} = \frac{2}{9} \cdot \frac{2}{9} = \frac{4}{81}$. The signature is composed of two oppositely charged leptons, two bottom jets and a large amount of missing transverse energy E_T due to two undetected neutrinos. These dileptonic final states offer the cleanest signature with two leptons having high transverse momentum, p_T, but suffer from the low branching ratio $\mathcal{B} = \frac{4}{81}$. Furthermore, the missing E_T originating from the neutrinos requires a very good knowledge of the entire detector.

Semileptonic Decay Channel In this case, one W boson decays hadronically, the other one leptonically. The branching ratio then is $\mathcal{B} = 2 \cdot \frac{2}{9} \cdot \frac{2}{3} = \frac{8}{27}$. Hence, the branching ratio is larger than the one of dileptonic events, however, there is more background. The signature consist of four jets altogether, two b jets next to two light jets from the W boson decay, one isolated and charged high p_T lepton and missing transverse energy E_T. Since just one neutrino is involved, its momentum can be reconstructed because of momentum and energy conservation.
For the analysis described in the next chapters, only such semileptonic $t\bar{t}$ decay events with four jets, one lepton and missing transverse energy in the final state are taken into consideration as the corresponding channel is a compromise between a high branching ratio and a small background.

3 The ATLAS Experiment

This bachelor thesis about different b-tagging methods, which help to improve the top quark reconstruction, has been performed within the ATLAS Collaboration. ATLAS is one of altogether four detector experiments, excluding two smaller ones, located at the Large Hadron Collider at CERN[1] in Geneva, which started operating at the end of 2009. This chapter deals with a short description of the LHC and the ATLAS detector, then some information concerning detector observables are presented.

3.1 The Large Hadron Collider

The Large Hadron Collider (LHC) is a proton-proton (pp) collider which was built in the former Large Electron Positron Collider (LEP) tunnel. The accelerator has a circumference of about 27 km and is situated approximately 100 m below the ground. During the next few years, the LHC will operate at a center-of-mass energy of $\sqrt{s} = 7$ TeV. After a shutdown period, the LHC will reach $\sqrt{s} = 14$ TeV at a design luminosity of 10^{34} cm^{-2}s^{-1}. Because of its high center-of-mass energy, the LHC can be used to look for new physics beyond the Standard Model, which will also be tested at a high precision.
In order to achieve the high intensities needed, the LHC accelerates the protons in two independent beam pipes with opposite magnet dipole fields. The particles are accelerated by radio frequency cavities with an ultrahigh vacuum of 10^{-10} mbar, situated inside the beam pipe. Dipole magnets are employed to keep the beams on their circular path while quadrupole magnets are essential for focusing the beams. When reaching its maximum energy, the LHC can store 2808 bunches in each beam with about 10^{11} protons in each bunch. A bunch crossing is expected every 25 ns.
The acceleration cavities as well as the guidance magnets of the LHC use supercon-

[1] European Organization for Nuclear Research, name originating from: Conseil Européen pour la Recherche Nucléaire

ducting technologies. The dipoles are cooled down to reach temperatures of about 1.9 K. Using superfluid helium allows for a maximum central field strength of 8-8.5 T to bend the colliding beams [19].
Before entering the LHC, all proton beams are pre-accelerated in a chain of older and smaller ring or linear accelerators at CERN that were upgraded to meet the requirements of the LHC.

Four experiments are located along the beam pipe of the LHC:
Two of four interaction sections host the high luminosity (10^{34} $cm^{-2}s^{-1}$) general-purpose detectors ATLAS and CMS. TOTEM, positioned near the CMS detector, measures the total cross section, elastic scattering and diffractive processes. LHCb, which aims at a peak luminosity of about 10^{32} $cm^{-2}s^{-1}$, concentrates on bottom quark physics while LHCf, positioned near the ATLAS detector, is used to measure the energy and number of neutral pions. ALICE with a luminosity of 10^{30} $cm^{-2}s^{-1}$ measures lead ions to produce a quark-gluon-plasma. Thus, conditions similar to those shortly after the so-called Big Bang can be achieved [20–22].

3.2 The ATLAS Detector

ATLAS (A Torodial LHC ApparatuS) is one of the two multi-purpose detectors at the LHC and is composed of several subdetectors. The main parts are an inner detector, two calorimeters, a muon spectrometer and a magnet system. Figure 3.1 gives an overview of the whole detector and the most important subsystems. ATLAS is about 44 m long and 25 m in diameter at a weight of approximately 7000 t [23].
The *inner detector* beginning a few centimeters from the beam axis consists of the *Pixel Detector*, the *Semi-Conductor Tracker* (SCT) and the *Transition Radiation Tracker* (TRT). The Pixel detector is composed of three layers and three disks on each side. There are over 80 million readout channels altogether providing a spatial resolution up to the order of a μm. Similar in concept and function is the so-called SCT which is made of long silicon strips instead of small pixels hence covering a larger area. There exist about 6.2 million readout channels. The detecting elements of the TRT are 351000 drift tubes (straws). These straw tubes are used to measure a particle's transition radiation which helps to determine their velocity. In this way, one can differentiate between several particles, e.g. electrons and pions.

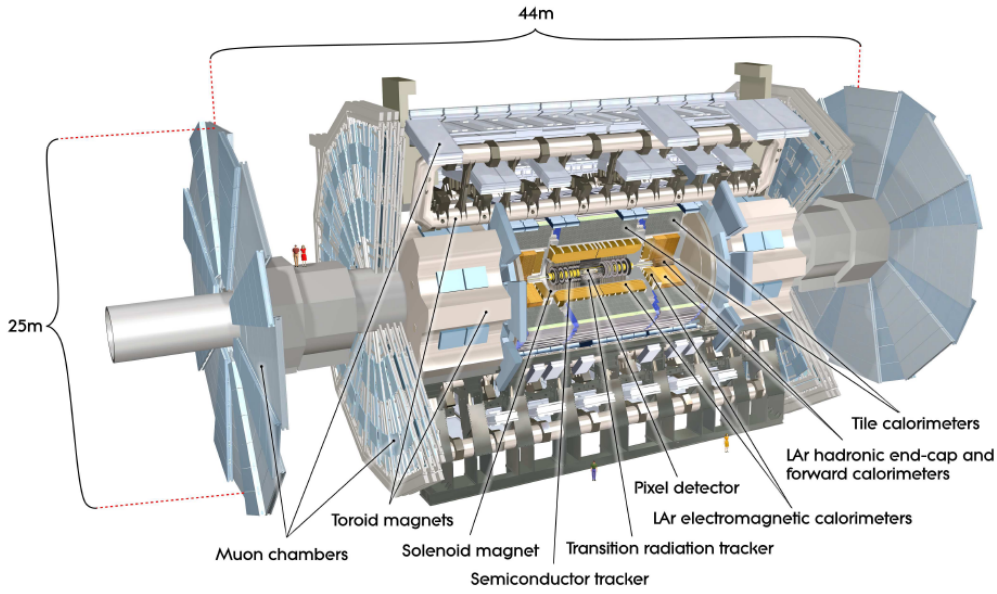

Figure 3.1: Cut-away view of the ATLAS detector and its subsystems [23].

The ATLAS experiment uses several kinds of *calorimeters* surrounding the inner detector. Basically, there are two calorimeter systems: an inner *electromagnetic calorimeter system* and an outer *hadronic calorimeter system*. Both are *sampling calorimeters*. In those calorimeters, passive absorber material and active material, attached to a read-out system, alternate [23]. In most ATLAS calorimeters liquid Argon serves as the active medium. The outer hadronic calorimeter, however, consists of scintillator tiles as the active medium and steel as the absorber. The calorimeter system absorbs the energy of particles in the detector so that the energy deposit of e.g. hadrons or leptons can be measured.

The *muon spectrometer* forms the outermost layer of the ATLAS detector. It detects muons leaving the calorimeters because they are minimum ionizing particles according to the Bethe-Bloch formula [3], measures its momentum and triggers on these particles. The spectrometer is composed of four differerent sorts of muon chambers arranged in a way that each incoming muon is detected by more than one chamber. That allows for the measurement of its momentum as well as its charge. The function of *Monitored Drift Tubes* (MDT) and *Thin Gap Chambers* (TGC) is the precision tracking of muons. The other two kinds of muon chambers are *Cathode Strip Chambers* (CSC) and *Resistive Plate Chambers* (RPC) which are both characterized by fast readout times and thus used for triggering. This will be

explored in depth later. Two large superconducting *magnet systems* are employed to bend charged particles in order to measure their momenta. The inner detector is surrounded by a *solenoid* producing a magnetic field of about 2 T. Outside the calorimeters and within the muon system, an outer *toroidal* magnetic field is located and produced by eight large air-core superconducting barrel loops and two end-caps. The trajectory of muons is bent by this inhomogeneous field of about 1 T.
Each bunch crossing generates extremely large amounts of data. Moreover, most detected events are expected to be less interesting QCD scattering events. For these reasons, a trigger system, in this case a three level one, is used, trying to identify, in real time, the most worthwhile events to retain for detailed studies [23].

3.3 Important Detector Observables

Usually, *cylindrical coordinates* (r, θ, ϕ) are used to describe positions inside the detector. r is the radial distance from the beam axis while ϕ is the so-called azimuthal angle. It specifies the direction which is perpendicular to the beam axis. Eventually, θ represents the angle between the particle's flight direction and the beam axis. Instead of the polar angle θ, the *pseudorapidity* is commonly used as the third coordinate. It depends on θ and is defined as follows [4]:

$$\eta = -\ln \tan \frac{\theta}{2}.$$

Differences in η are invariant under Lorentz boosts. A second advantage of using this quantity is the enormous rise of η in the detector region close to the beam axis as this area naturally contains a higher particle density. Thus, the separation between several particles is easier because distributions are flattened. Frequently, distances ΔR are specified in the η-ϕ-plane according to:

$$\Delta R = \sqrt{\Delta\phi^2 + \Delta\eta^2}.$$

This equation, which contains the differences $\Delta\phi^2$ and $\Delta\eta^2$ between the two objects in η and ϕ, is used in the later analysis.

4 Fundamentals of b-Tagging

4.1 Why b-Tagging?

As already mentioned in the introductory chapter, measurements of the top quark properties are a field of strong interest. A requirement for these measurements is an adequate reconstruction of the top quark decays, which will also be observed by the ATLAS detector as it was declared in the previous chapter. Chapter 2 offered an explanation why $t\bar{t}$ decays are relevant for top quark studies. In general, the decay of both top quarks forming such a pair leads, firstly, to two bottom quarks from which two jets in the detector originate and, secondly, to two W bosons which may decay hadronically into two lighter quarks that form two further jets due to hadronization. The W boson may also decay into leptons. Thus, there are zero, two or four jets altogether, depending on the W decay. In the following, the emphasis is put on semileptonic events as also stated in Chapter 2.
As a consequence, all considered events are characterized by four jets, which complicates the identification of both b jets, the so-called **b-tagging**. However, an identification of b jets is essential for reducing the background and for reconstructing the top quark decays, which is, in turn, needed for a precise measurement of the top quark properties. Accordingly, a better b-tagging efficiency means an improvement of the evaluation of the top quark properties. That is why b-tagging methods, being presented subsequently, are so useful.

4.2 Different Methods of b-Tagging

Jets originating from bottom quarks possess several unique properties that allow for a differentiation between these b jets and those coming from the hadronization of lighter quarks. Jets from u, d and s quarks hadronize directly at the *primary vertex*, the original interaction point. b jets contain B mesons, which may have a decay vertex displaced from the primary one, due to the comparatively long lifetime

of about 1.5 ps leading to a measurable flight length path of a few millimeters on average. That is why the decay of B hadrons can then take place at a *secondary vertex* [24].
The differentiation between b jets and light jets is typically based on the existence of such a secondary vertex. A bottom jet can be identified by measuring the *impact parameters* of tracks belonging to the decay. The impact parameter (IP) is defined as the distance from the closest approach of the track to the primary vertex. The IP can have different signs. It is selected positive if, with regard to the jet's propagation direction, the point of closest approach is located upstream and negative in the other case. Lying "upstream" corresponds to the case that the track crosses the jet axis, which can be seen in Fig. 4.1. Because of the existence of a secondary vertex, b jets tend to have a positive impact parameter rather than a negative one which facilitates the tagging of b jets. Additionally, identifying b jets via an explicit reconstruction of the secondary vertex, inclusively or exclusively, is possible as well [24]. Finding a lepton near a jet is also another indication for a b jet since the branching ratio of semileptonic B hadron decays is about 11% and hence considerably larger than the one of light hadrons due to the long lifetime of B hadrons and the Lorentz boost.

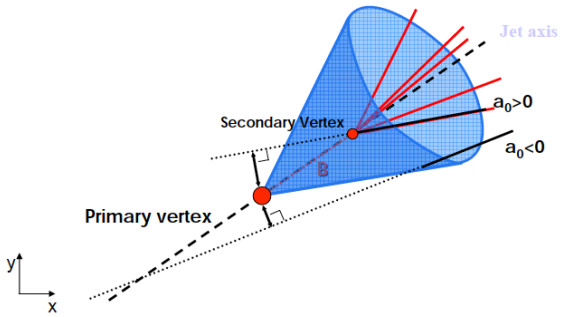

Figure 4.1: Illustration of the secondary vertex, displaced from the primary one, and of the sign of the impact parameter a_0 in the transverse projection. "B" represents a B meson.

The different algorithms with which b jets are identified are called *taggers*. The simplest ones just tag a jet as a bottom jet if a certain number of tracks belonging to the jet have an impact parameter that exceeds a fixed value or if the B hadron's flight distance significance, depending on the secondary vertex position, is larger than a certain cut value.
Improved taggers are, for example, the *IPxD* taggers. These use the impact param-

eter as well as the IP significance which is defined as [25]:

$$S = \frac{\mathrm{IP}}{\sigma_{\mathrm{IP}}}.$$

The *IP1D* tagger is based on the impact parameter in the longitudinal projection z_0, that is the IP in jet direction, whereas the *IP2D* tagger utilises the IP a_0 in the transverse projection. A combination of these two taggers is called *IP3D* depending on both z_0 and a_0. For the separation of b jets and lighter jets, an additional discriminating variable is introduced, the *jet weight*. If the tagger *IP3D* is used, the jet weight W_{jet}^{3D} depends on two-dimensional track significance probability functions which are obtained from calibration histograms. Then, all jets having a jet weight above a certain cut value $W_{\mathrm{cut}}^{\mathrm{bjet}}$ are tagged as bottom jets:

$$W_{\mathrm{jet}}^{3D} > W_{\mathrm{cut}}^{\mathrm{bjet}}. \tag{4.1}$$

Other sophisticated taggers are based on the reconstruction of the secondary vertex, such as the *SV1/2* tagger. These calculate the jet weight by using several one or more dimensional variable distributions, for example, vertex mass, energy fraction of the tracks fitted to the considered vertex, in comparison to all tracks in the jet, or the angle between jet direction and B hadron flight direction. The appropriate jet weight W_{jet}^{SV} also includes the ratio of probability functions for b jets and lighter jets [24].
Moreover, some commonly used soft-lepton taggers are also employed. One, for example, uses muons and a reference histogram of their transverse momenta.
In some cases several more advanced taggers are merged, which means the combination of the jet weights of various taggers in order to reach a better discrimination between b and light jets. In this thesis, an *IP3DSV1* tagger is utilized, that is, in accordance with its name, a combination of an *IP3D* and a *SV1* tagger.
In order to estimate the quality of this tagger, a *b-tagging efficiency* ε_b can be calculated, determined by the specific cut value $W_{\mathrm{cut}}^{\mathrm{bjet}}$. The efficiency is defined as the fraction of b jets that are correctly tagged as b jets while the so-called *rejection* R_l is defined as the inverse of the fraction of light jets that are falsely tagged as b jets:

$$\varepsilon_b = \frac{N(b|\text{tag } b)}{N(b)} \qquad \text{and} \qquad R_l = \frac{N(l)}{N(l|\text{tag } b)}.$$

Thus, a high efficiency as well as a high rejection is required. $N(b)$ and $N(l)$ are

the numbers of b jets and light jets, "tag b" refers to jets which fulfill the b-tagging criteria. Both, efficiency and rejection, usually depend on η and on the transverse momentum p_T of the jet [24].
In the following, jets referred to as "light jets" not only include u, d and s quarks, but also c quarks are considered although, to a certain extent, their properties are similar to those of b quarks.

In this thesis, different methods of helping to improve the b-tagging efficiency are implemented in the *Kinematic Likelihood Fitter*, a program which is described in a more detailed way in the next chapter.

5 Kinematic Fitting

The KLFitter, short for *Kinematic Likelihood Fitter*, is a tool for kinematic fitting using a likelihood approach, based on ROOT in C++ [26]. It puts emphasis on the description of the energy resolution of the objects in the final state which are, for example, jets or leptons. The tool's features are described for semileptonic $t\bar{t}$ events as these events are essential for the studies done in this thesis. Therefore, the KLFitter can be defined as a tool for the reconstruction of top-antitop quark pairs in semileptonic decays. In the previous chapter, b-tagging as a possibility of improving the top quark reconstruction was introduced. The main aim of this thesis is to add several b-tagging methods to the KLFitter in order to advance this tool by gaining an increase in the efficiency of identifying b jets correctly and, consequently, also in the top quark reconstruction efficiency.
In this chapter some background information about kinematic fitting and the sample which is used for the studies are presented. Furthermore, an explanation concerning the analysis of the KLFitter output file is given.

5.1 Kinematic Fitting with the KLFitter

Since this kinematic fitting is based on a likelihood approach, it is necessary to concentrate on the likelihood at first. The likelihood is defined as the probability for observing a set of measured quantities which are given by a model with a corresponding set of parameters. The probability is calculated in accordance with the model. For the studies presented here, semileptonic decays with a final state consisting of four jets, one lepton and the corresponding neutrino are assumed.
The following quantities from the measurement are considered: The energies and directions of all four jets belonging to the $t\bar{t}$ decay, $\tilde{E}_i$ and $\tilde{\Omega}_i = (\eta_i, \phi_i)$ with $i = 1, ..., 4$, the energy and direction of the charged lepton, $\tilde{E}_{\text{lep}}$ and $\tilde{\Omega}_{\text{lep}}$, and the missing transverse energy, E_T^{miss}, due to the neutrino. The direction of the lepton is expected to be measured precisely. However, the energies of quarks and leptons as well as the

directions of the four quarks cannot be measured accurately which leads to some uncertainty given by the corresponding energy and angular resolution, parametrized by so-called *transfer functions* $W(\tilde{E}_i, E_i)$ and $W(\tilde{\Omega}_i, \Omega_i)$, $i = 1, ..., 4$. The first ones, depending on the energy, map the measured energy of an object to the energy of the final state particles, the other ones, depending on the direction, map the measured angles of an object to the angles of the final state particles.
The calculation of the likelihood is based on several assumptions:

- The transfer functions $W(\tilde{E}, E)$ of all quark and the charged lepton energy as well as the transfer functions $W(\tilde{\Omega}, \Omega) = W(\tilde{\eta}, \eta) \cdot W(\tilde{\phi}, \phi)$ of all quark angles are known.

- The transfer functions $W(E^{\text{miss}}_{x/y}, p^{\nu}_{x/y})$ of the neutrino momentum are also known. This applies to the two components x and y of the neutrino momentum because the corresponding transverse momentum can be estimated from the missing transverse momentum as neutrinos do not interact with the detector.

- The masses of both the hadronically and leptonically decaying W bosons, m_{jj} and $m_{\ell\nu}$, are distributed in accordance to a Breit-Wigner distribution BW around a pole mass of $M_W = 80.4\ \frac{\text{GeV}}{c^2}$.

- The masses of the two top quarks, m_{jjj} and $m_{\ell\nu j}$, are distributed according to a Breit-Wigner distribution BW as well. The masses are spread around the top pole mass, which is, for these studies, an additional free parameter.

Thus, there are 17 fit parameters altogether: The energies E_i and the directions Ω_i of all four quarks (12 parameters), the energy of the charged lepton E_ℓ (one parameter), the momentum of the neutrino $\vec{p}^{\,\nu}$ (3 parameters) and the top pole mass M_{top} (one parameter).
The parameter ranges depend on each event. All involved energies have to be within a range around the measured values: $\min(0, \tilde{E} - n \cdot \sqrt{\tilde{E}}) < E < \tilde{E} + n \cdot \sqrt{\tilde{E}}$ with $n = 7$ for jets or partons and $n = 2$ for leptons. The x- and y-component of the neutrino are assumed to be within a range of $\pm 100\ \frac{\text{GeV}}{c}$ around the measured missing transverse momentum, the z-component within a range of $\pm 1000\ \frac{\text{GeV}}{c}$. Finally, the η- and ϕ-angles are assumed to be within a range of ± 0.2 and ± 0.1 around the measured angles whereas the top pole mass is expected to be between $100\ \frac{\text{GeV}}{c^2}$ and $400\ \frac{\text{GeV}}{c^2}$.

The likelihood function L with Breit-Wigner functions $BW(a|b)$ centered around b then is:

$$L = \left(\prod_{i=1}^{4} W(\tilde{\Omega}_i, \Omega_i)\right) \cdot \left(\prod_{i=1}^{4} W(\tilde{E}_i, E_i)\right) \cdot W(\tilde{E}_l, E_l) \cdot W(E_x^{\text{miss}}|p_x^{\nu}) \cdot W(E_y^{\text{miss}}|p_y^{\nu}) \cdot \\ \cdot BW(m_{jj}|M_W) \cdot BW(m_{\ell\nu}|M_W) \cdot BW(m_{jjj}|M_{\text{top}}) \cdot BW(m_{\ell\nu j}|M_{\text{top}}). \quad (5.1)$$

Since an association of jets with the four different quarks is not feasible in the first place, all possible ways of association have to be considered. As there are four jets, $4! = 24$ permutations of jets have to be taken into account in order to associate jets with quarks. But the likelihood is symmetric under the permutation of the two jets belonging to the quarks from the hadronic W boson decay. Hence, only 12 permutations of jets need to be considered leading to 12 likelihood functions for each event. In this thesis, each permutation will also be weighted with b-tagging jet weights as explained in Chapter 4. Such an implementation simplifies the assignment of a b quark to a certain jet. The invariant mass of jets associated with the two light quarks is supposed to be within a range of $40\frac{\text{GeV}}{c^2} - 120\frac{\text{GeV}}{c^2}$. Otherwise such a permutation is excluded from the fit, as well as permutations for which a minimum could not be determined.
Instead of the likelihood function, the function $-\ln L$ is minimized with regard to the parameters for each permutation. For this modelling, the BAT package is used where the minimization is realized with the interface to Minuit [27]. The measured values for all energies, the invariant masses as well as the angles are used as starting values while the z-component of the neutrino momentum needs to be calculated from the initial values; the starting value is the solution giving the larger likelihood. In the end, the fitter returns the best fit parameters and the corresponding value of the likelihood function, which is referred to as $-\ln L^*$, as well as a relative weight for each jet permutation. These are ordered in accordance to their relative weights built from $-\ln L^*$ and b-tagging weights in a way that the sum of relative weights is normalized to unity. That combination which gives the highest value for the Likelihood is labelled as being the best permutation. However, this is not necessarily the true combination.

The KLFitter package is built in a modular way. The class structure can be described as follows:
The central class is the “Fitter” class which contains objects that characterize the

detector (an instance of "DetectorBase"), all input particles (an instance of "Particles"), the likelihood (an instance of "LikelihoodBase") and an additional instance of "Permutations" allowing for managing the possible permutations of jets to quarks. The DetectorBase class contains the detector information whereas the Particle class provides containers for different types of particles. The fitting procedure is done in the LikelihoodBase class which inherits from the BAT libraries.

5.2 Monte Carlo Data Sample

The studies presented in this thesis are performed on a certain Monte Carlo (MC) data sample saved as a ROOT-file. It contains events with both dileptonic and semileptonic final states and is obtained from the Monte Carlo generator MC@NLO [28, 29] which can be described as a next-to-leading order Monte Carlo event generator. The events were generated at a center-of-mass energy of 7 TeV and a top pole mass of 172.5 $\frac{\text{GeV}}{c^2}$ then passed to the ATLAS simulation software and reconstructed by using the ATHENA framework [30]. The total number of events in the sample is 61,969, the corresponding ROOT-tuple was created by the use of GoTopTree, a private n-tuple maker of the Göttingen top group.
In creating the sample, the following object definitions are used:

- Only electrons with $p_T > 15\frac{\text{GeV}}{c}$ and $|\eta| < 2.47$, excluding the crack-region, are considered.

- Jets, which are reconstructed by an anti-k_t algorithm [31] with a size, which equals the radius in the η-ϕ-space, of 0.4 need to have $p_T > 15\frac{\text{GeV}}{c}$ and $|\eta| < 2.5$.

- The missing E_T is defined as MET_RefFinal.

The so-called "crack-region" ($1.37 \leq \eta \leq 1.52$) is the border between the barrel and forward calorimeters in a detector. Electrons in this region cannot be reliably reconstructed and are consequently excluded.
In addition, jets which overlap with electrons are removed if their distance in η-ϕ-space, as explained in Chapter 3.3, is $\Delta R = \sqrt{\Delta\phi^2 + \Delta\eta^2} < 0.2$, a necessary removal as the jet algorithm reconstructs most electrons as jets.

Pre-Selection From this point on, only events in the semileptonic decay channel with electrons as leptons in the final state are taken into account. On truth level, a pre-selection is applied where events are required to have two b and two light jets as well as one electron in the truth container. Furthermore, the event must contain at least one electron and one jet.

Event Selection The following list presents the event selection criteria similar to those in the CSC-notes [32]. Each event passing the criteria contains:

- One electron with $p_T > 20 \ \frac{\text{GeV}}{c}$ and $|\eta| < 2.5$.
- 3 jets with $p_T > 40 \ \frac{\text{GeV}}{c}$ and $|\eta| < 2.5$.
- One additional jet with $p_T > 20 \ \frac{\text{GeV}}{c}$ and $|\eta| < 2.5$.
- Missing transverse energy with $E_T^{\text{miss}} \geq 20$ GeV.

The four leading jets, with regard to p_T, are associated with the top quark pair and used for the calculation of the likelihood while all other jets are ignored.

Matching Finally, it is often essential to identify jets with the associated quark from the leading order hard scattering process. This identification succeeds with the help of a geometric matching criterion based on the distance ΔR between jet and quark in the η-ϕ-space. Two objects are regarded as matched if $\Delta R = \sqrt{\Delta\phi^2 + \Delta\eta^2} < 0.3$. On the basis of this definition, an event is referred to as matched if the four selected jets could be matched to the four final state partons of the hard scattering process and if the lepton candidate is identified with the truth lepton. The number of remaining and thus matched events in the sample is important for estimating the total efficiency of the KLFitter.

Incidentally, the transfer functions, as mentioned in Section 5.1, are derived from the Monte Carlo sample, or more precisely, they are derived from reconstructed objects matched to the corresponding truth particles and fulfilled the matching requirements. The functions are then parametrized by double Gaussians.

5.3 Output Files

The KLFitter output file includes several ROOT trees. The tree "Truth" contains the Monte-Carlo-generated events, the tree "Measured" the values being produced by smearing the generated jet energies (from light and b quarks) in accordance with a Gaussian distribution. The tree "Selected" includes the particles selected for the fit, the results of this fit can be found in the tree "Model" while the tree "Map" contains the mapping between both measured and selected particles. All fitted variables are written into arrays with 12 entries, one for each permutation.
With an additional program, also based on ROOT, a so-called *Top Histogram Maker*, the following efficiencies can be evaluated: The efficiencies of reconstructing the whole top-antitop quark pair decay and of identifying the hadronic W boson or both b quarks as well as the b-tagging efficiency. The latter is the probability of tagging a b quark correctly. Moreover, the fraction of light quarks falsely identified as b jets can be calculated. Generally, the efficiency of identifying a certain particle A is defined as the fraction of particles A that are properly tagged. Accordingly, the reconstruction efficiency is the fraction of events that are correctly reconstructed.

6 Results

In this chapter, the studies done to improve the top quark reconstruction efficiency, implying a more precise measurement of the top quark properties, as well as their results are presented. This can be achieved by implementing various b-tagging methods in the KLFitter.
At first, the different efficiencies which can be calculated with the help of the KLFitter output file are analyzed in the case that no b-tagging is used. These data will serve as reference material and comparable data for subsequent tests. Two different b-tagging methods are then presented and their results including the improvements concerning the efficiencies which can be achieved by using these methods, are discussed. It is focused on the determination of the *b-tagging efficiency* and the *reconstruction efficiency*. Both methods depend on a jet weight distribution, one uses jet weight cut values, the other method is based on the shape of the jet weight distribution. For these studies, all events passing the event selection criteria, pre-defined in Section 5.2, are chosen.
Finally, next to the *reconstruction efficiency*, the *matching efficiency* can be taken into account as not all events passing the event selection criteria and being used for the top quark reconstruction fulfill the matching criterion, also defined in Section 5.2. Both reconstruction and matching efficiency can be combined which leads to the *total efficiency* calculated within the framework of a supplementary analysis described in the last section.
With the Top Histogram Maker, all given efficiencies including the errors are calculated. The latter are rounded to three significant digits allowing for an easier comparison between those efficiencies which originate from different KLFitter versions.

6.1 Top Quark Reconstruction without b-Tagging

The KLFitter was introduced as a tool for kinematic fitting which is based on a likelihood approach. As a first test, the KLFitter is run without any kinematic fitting. In that case, the different KLFitter efficiencies, which are listed in Chapter 5.3 and which correspond to the probabilities P for the correct identification of a jet or a particle, can be gained from pure statistics. Theoretically, the following probabilities are expected:
Since the combinations with interchanged light quarks are counted once, there are altogether 12 permutations of jets to associate jets with quarks. Thus, in one of twelve cases the true combination is found and all four jets are correctly identified, $P(\text{all correct}) = \frac{1}{12} \approx 8.33\%$. The hadronic W boson can be properly reconstructed in two ways as interchanging the two b quarks does not influence the W momentum $p_W = p_{q1} + p_{q2}$ so that $P(W_{\text{had}} \text{ correct}) = \frac{2}{12} \approx 16.67\%$. If either the hadronic or the leptonic b quark is labelled correctly, the remaining three jets can be commuted among themselves. Consequently, $\frac{3!}{2}$ permutations result in a right mapping of the hadronic (or leptonic) b quark with a probability of $P(b_{\text{lep/had}} \text{ correct}) = \frac{3}{12} = 25\%$ in each case.
Furthermore, the b-tagging probability can be estimated, taking into consideration that the leptonic b jet can be characterized as the hadronic one and vice versa. Hence, as two of four jets are b jets, the probability to tag a true b jet as a b jet, in other words the b-tagging probability, is $P(b \text{ tag} \mid \text{truth } b) = \frac{2}{4} = 50\%$ that equals the b-tagging efficiency ε_b of the KLFitter. The probability of identifiying a jet as a b jet, although it is in fact a light jet, is accordingly $P(b \text{ tag} \mid \text{light } q) = \frac{2}{4} = 50\%$.
The results which can be gained from the KLFitter, if kinematic fitting is deactivated, are listed in Table 6.1. As expected, they resemble the ones just calculated with the help of pure statistics, which, for comparison, can also be found in Table 6.1.
However, there are some differences between the two values obtained from the KLFitter and from pure statistics although the ones originating from the KLFitter have comparatively small errors. This is due to the correlation between the different efficiencies. Consequently, the attached uncertainties and errors are correlated as well, possibly causing an underestimation of the listed errors.

Before implementing the b-tagging methods, the version of the KLFitter, where

Probability/ Efficiency	Pure combinatorics	KLFitter - no kin. fitting	KLFitter
P(all correct) [%]	8.33	5.68 ± 0.41	50.32 ± 1.21
$P(W_{\text{had}}$ correct) [%]	16.67	14.12 ± 0.65	57.86 ± 1.30
$P(b_{\text{had}}$ correct) [%]	25.00	25.07 ± 0.86	54.29 ± 1.26
$P(b_{\text{lep}}$ correct) [%]	25.00	20.25 ± 0.78	74.74 ± 1.48
$P(b$ tag $\mid$ truth $b)$ [%]	50.00	49.45 ± 1.21	77.70 ± 1.51
$P(b$ tag $\mid$ light $q)$ [%]	50.00	50.55 ± 1.23	22.30 ± 0.81

Table 6.1: Different efficiencies of the KLFitter if b-tagging methods are not implemented.

kinematic fitting is activated, is tested as well. As Table 6.1 reveals, all efficiencies increase, in comparison with the version described above, except for the fraction of light quarks falsely identified as b jets, which decreases, thus showing the assumed and desired behaviour. The reconstruction efficiency reaches $\varepsilon_R \approx 50\%$ which indicates the quality of the kinematic fitting as ε_R is less than 10% if the latter is not used. The b-tagging efficiency ε_b even increases to almost 78%. Hence, kinematic fitting is a vital tool for the reconstruction of top quark pair decays. However, with the use of b-tagging, further improvement concerning the efficiencies is feasible as being presented in the following sections.
Fig. 6.1 clearly visualizes the different efficiencies or probabilities listed in Table 6.1.

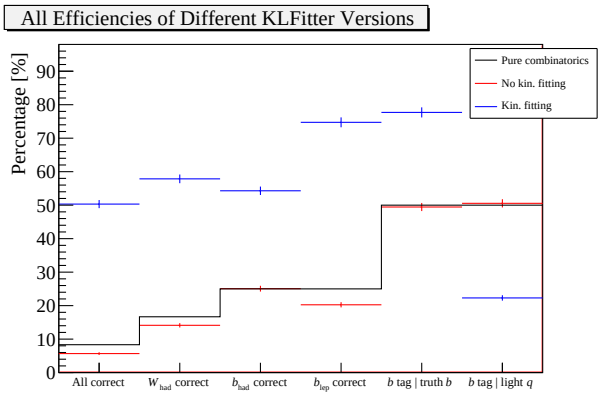

Figure 6.1: Plot for the different efficiencies of the KLFitter if b-tagging methods are not implemented.

6.2 b-Tagging with Cut Values

Both b-tagging methods described and analyzed in this thesis are based on jet weights. For all jets which are included in the sample a jet weight can be calculated. In this case, this is done by an *IP3DSV1* algorithm, as pre-defined in Chapter 4, using the impact parameter and the reconstruction of the secondary vertex. All jet weights can be obtained from the KLFitter input file which also contains all MC events. As the truth information is available, a differentiation between jet weights originating from B jets or from lighter jets (u, d, s and c) can be realized.
The truth information provides the detector coordinates η and ϕ for all b quarks in the sample. Then the differences $\Delta\eta$ and $\Delta\phi$ between all jets of the event to which a certain b quark belong and the quark itself can be calculated. If both, quark and jet, fulfill the matching criterion $\Delta R = \sqrt{\Delta\phi^2 + \Delta\eta^2} < 0.3$, the jet is in fact a b jet and the corresponding jet weight obtained from the *IP3DSV1* tagger is the weight of a b jet. In this way, all jet weights belonging to b jets can be separated from those belonging to all other (lighter) jets. Accordingly, a jet weight distribution for lighter jets as well as for b jets can be determined. Both distributions are presented in Fig. 6.2.

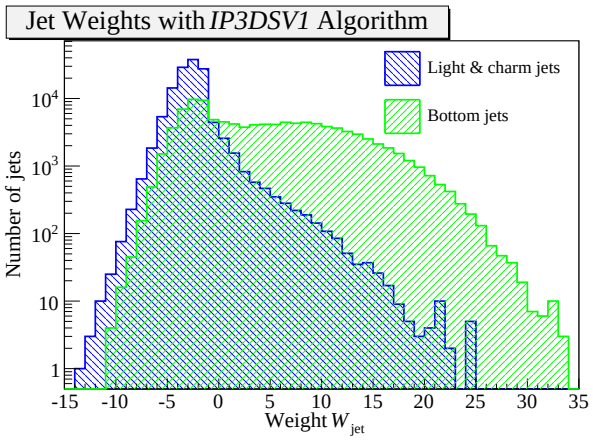

Figure 6.2: Both jet weight distributions for either b jets (green) or light jets (including c jets) (blue). The weights are calculated by an *IP3DSV1* algorithm.

Because of the comparatively high peak around -2, a logarithmic scale is used. The plot reveals that the distribution of b jets is shifted to larger values, lighter jets tend to have smaller weights, especially more often negative ones. The large b jet weights are caused by a long-lived B meson which is responsible for more b jets having a positive impact parameter than light jets and which may lead to a secondary vertex.

This is due to the fact that the IP is positive if, with regard to the jet's propagation direction, the track's point of closest approach to the primary vertex lies upstream (see Fig. 4.1) which arises more frequently if a secondary vertex exists.
The differences in the appearance of both distributions can be utilized for b-tagging. As the jet weights of b jets, W^b_{jet}, reveal the tendency of being larger than jet weights of lighter jets, W^l_{jet}, a jet is tagged as a b jet if its weight exceeds a certain value, the so-called *cut value* $W^{\text{bjet}}_{\text{cut}}$. Thus, a jet with jet weight W_{jet} is tagged as a b jet if

$$W_{\text{jet}} > W^{\text{bjet}}_{\text{cut}}, \tag{6.1}$$

otherwise it is tagged as a light jet. The cut value can be chosen arbitrarily. This inequation resembles the rule which was introduced to describe the more simple tagger *IP3D* (see Equation (4.1)), formally deduced in the last few lines.

This first b-tagging method, referred to as the "cut method", is added to the original version of the KLFitter. The jet weights of all jets in the sample are compared with the chosen cut value according to Inequation (6.1) and then the corresponding jet is either tagged as a b jet or as a light jet depending on the particular jet weight.
The likelihood function, defined in Equation (5.1), is calculated for all twelve permutations belonging to an event. In the case of b quarks, according to the theoretical quark position in the permutation, the likelihood function L is multiplied by "1" if the corresponding jet weight exeeds the cut value. The likelihood function is multiplied by "0" if a jet is regarded to be a light one, compliant with the position of the associated quark in the permutation, although the jet is tagged as a b jet due to its large weight.
Pursuant to the shape of both jet weight distributions (see Fig. 6.2), cut values between zero and ten, $0 \leq W^{\text{bjet}}_{\text{cut}} \leq 10$, seem to be most suitable for an appropriate and correct identification of b and light jets. This is due to the fact that chosing a certain cut value merely represents an approximation. If $W^{\text{bjet}}_{\text{cut}} > 10$, a comparatively large amount of b jets is tagged as light jets and if $W^{\text{bjet}}_{\text{cut}} < 0$, large quantities of light jets are tagged as b jets. Thus, it becomes obvious that not only a high b-tagging efficiency ε_b is relevant, a high light jet rejection R_l, as defined in Chapter 4, is preferable as well.
The results for the different efficiencies for all chosen cut values are listed in Table 6.2. As mentioned above, all given probabilities equal the efficiencies of identifying the

corresponding particle correctly.

Probability/Efficiency	No b-tag.	$W_{\text{cut}}^{\text{bjet}} = 0$	$W_{\text{cut}}^{\text{bjet}} = 1$	$W_{\text{cut}}^{\text{bjet}} = 2$
P(all correct) [%]	50.32 ± 1.21	63.04 ± 1.36	64.51 ± 1.37	65.14 ± 1.38
$P(W_{\text{had}}$ correct) [%]	57.86 ± 1.30	73.50 ± 1.47	75.33 ± 1.48	75.91 ± 1.49
$P(b_{\text{had}}$ correct) [%]	54.29 ± 1.26	67.51 ± 1.40	68.31 ± 1.41	68.70 ± 1.42
$P(b_{\text{lep}}$ correct) [%]	74.74 ± 1.48	75.05 ± 1.48	76.76 ± 1.50	77.69 ± 1.51
P(b tag | truth b) [%]	77.70 ± 1.51	86.06 ± 1.59	87.09 ± 1.60	87.47 ± 1.60
P(b tag | light q) [%]	22.30 ± 0.81	13.94 ± 0.64	12.91 ± 0.61	12.53 ± 0.60
Probability/Efficiency	$W_{\text{cut}}^{\text{bjet}} = 3$	$W_{\text{cut}}^{\text{bjet}} = 4$	$W_{\text{cut}}^{\text{bjet}} = 5$	$W_{\text{cut}}^{\text{bjet}} = 6$
P(all correct) [%]	64.48 ± 1.37	64.01 ± 1.37	63.35 ± 1.36	62.80 ± 1.35
$P(W_{\text{had}}$ correct) [%]	75.01 ± 1.48	74.57 ± 1.47	73.72 ± 1.47	72.83 ± 1.46
$P(b_{\text{had}}$ correct) [%]	67.60 ± 1.40	67.28 ± 1.40	66.82 ± 1.40	66.24 ± 1.39
$P(b_{\text{lep}}$ correct) [%]	78.05 ± 1.51	78.22 ± 1.51	78.36 ± 1.51	78.03 ± 1.51
P(b tag | truth b) [%]	87.04 ± 1.59	86.92 ± 1.59	86.51 ± 1.59	85.98 ± 1.58
P(b tag | light q) [%]	12.96 ± 0.62	13.08 ± 0.62	13.49 ± 0.63	14.02 ± 0.64
Probability/Efficiency	$W_{\text{cut}}^{\text{bjet}} = 7$	$W_{\text{cut}}^{\text{bjet}} = 8$	$W_{\text{cut}}^{\text{bjet}} = 9$	$W_{\text{cut}}^{\text{bjet}} = 10$
P(all correct) [%]	61.55 ± 1.34	60.23 ± 1.33	58.98 ± 1.31	57.95 ± 1.30
$P(W_{\text{had}}$ correct) [%]	71.15 ± 1.44	69.49 ± 1.43	68.13 ± 1.41	66.89 ± 1.40
$P(b_{\text{had}}$ correct) [%]	65.14 ± 1.38	63.94 ± 1.37	62.78 ± 1.35	61.95 ± 1.35
$P(b_{\text{lep}}$ correct) [%]	77.72 ± 1.51	77.41 ± 1.50	77.25 ± 1.50	76.71 ± 1.50
P(b tag | truth b) [%]	85.02 ± 1.58	84.16 ± 1.57	83.48 ± 1.56	82.82 ± 1.56
P(b tag | light q) [%]	14.98 ± 0.66	15.84 ± 0.68	16.52 ± 0.70	17.18 ± 0.71

Table 6.2: Efficiencies of the KLFitter for various cut values $W_{\text{cut}}^{\text{bjet}}$. The results obtained from the original KLFitter version are listed as well.

In order to compare these efficiencies with the ones of the original version of the KLFitter, the associated numbers are also given. As expected, with the help of this b-tagging method, the b-tagging efficiency ε_b increases and, as a consequence, all other important efficiencies of identifying particles accurately, calculated by the Top Histogram Maker, as well, depending on the associated cut value. Especially the reconstruction efficiency ε_R increases. As it can be seen in Table 6.2, the cut value $W_{\text{cut}}^{\text{bjet}} = 2$ leads to the highest efficiencies. ε_R reaches almost 65% while ε_b rises to 87%. Compared to the original version of the KLFitter with $\varepsilon_R \approx 50\%$ and $\varepsilon_b \approx 78\%$, respectively, the increase in the efficiency is quite considerable indicating the importance of b-tagging in the case of a reconstruction of top quark decays.
In Fig. A.3 and A.4 in the Appendix, the efficiencies are also presented in several plots, one for each cut value. Figure 6.3 shows the reconstruction as well as the b-tagging efficiencies for all tested cut values. The peak at $W_{\text{cut}}^{\text{bjet}}$ is visible, but all

cut values in the range of $W_{\text{cut}}^{\text{bjet}} = 1$ to $W_{\text{cut}}^{\text{bjet}} = 4$ offer comparatively adequate results.

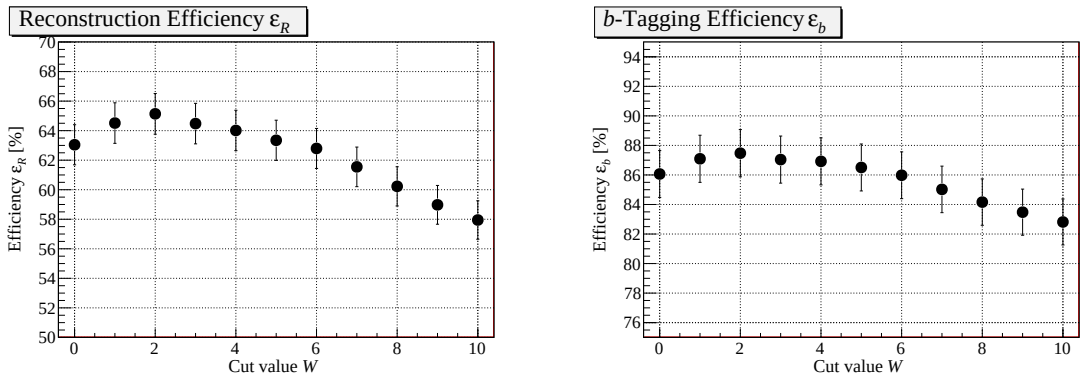

Figure 6.3: Reconstruction efficiencies (left) and b-tagging efficiencies (right) for all tested cut values, $0 \leq W_{\text{cut}}^{\text{bjet}} \leq 10$, with $W_{\text{cut}}^{\text{bjet}} \hat{=} W$.

The efficiencies decrease appreciably for $W_{\text{cut}}^{\text{bjet}} > 5$, except for the probability of identifying the hadronic b quark correctly, which is nearly constant and reaches its maximum at $W_{\text{cut}}^{\text{bjet}} = 5$. The efficiencies for even larger cut value in the examined range still exceed the ones originating from the former version of the KLFitter, however, they cannot reach the high values obtained from the just mentioned best cut values.

In Chapter 6.1, the efficiencies of the KLFitter were calculated in the case that no kinematic fitting is used and in the case that no additional b-tagging method is implemented. Supplementary, a version of the KLFitter can be tested which depends on the b-tagging method based on cut values instead of on any kinematic fitting. The results, if the "best" cut value $W_{\text{cut}}^{\text{bjet}} = 2$ is chosen, can be seen in Table 6.3. To compare the values, the results of the KLFitter versions from Section 6.1 are listed as well. As expected, the b-tagging efficiency $\varepsilon_b = P(\text{b tag} \mid \text{truth b})$ of the now tested KLFitter version offers quite adequate values as it surpasses the one of the original KLFitter version which do not use b-tagging, 81% compared to 78%. But since no kinematic fitting is used, all other efficiencies just depend on ε_b. Consequently, especially the probabilities of identifying the hadronic or the leptonic b quark properly are quite low as these values are only half as large as the b-tagging probability. Thus, also the reconstruction efficiency is lower as well, 31% compared to 50%, because the probability of identifying all jets correctly is just based on the

Probability/ Efficiency	KLFitter - no kin. fit./no b-tag.	KLFitter - kin. fitting only	KLFitter - b-tagging only
P(all correct) [%]	5.68 ± 0.41	50.32 ± 1.21	31.80 ± 0.97
$P(W_{\text{had}}$ correct) [%]	14.12 ± 0.65	57.86 ± 1.30	63.27 ± 1.37
$P(b_{\text{had}}$ correct) [%]	25.07 ± 0.86	54.29 ± 1.26	38.10 ± 1.06
$P(b_{\text{lep}}$ correct) [%]	20.25 ± 0.78	74.74 ± 1.48	41.99 ± 1.12
P(b tag | truth b) [%]	49.45 ± 1.21	77.70 ± 1.51	80.95 ± 1.55
P(b tag | light q) [%]	50.55 ± 1.23	22.30 ± 0.81	19.05 ± 0.75

Table 6.3: Different efficiencies of the KLFitter in the case that no kinematic fitting or no b-tagging is implemented.

b-tagging information.

As stated in Chapter 5.2, the sample used for these studies contains 61,969 events. 16,466 top quark decays can be used for fitting. When reconstructing those top quark pair decays, the KLFitter is not always able to tag two b jets per event since this tagging depends on the chosen cut value. Hence, a further differentiation between events with no tagged b jets, one tagged b jet and events with two tagged b jets can be implemented.
This distinction is realized with the help of a quantity which can be found in the KLFitter output file, the *Event Probability* (EP), which is the relative likelihood value compared to the sum of all other permutations. As twelve different permutations have to be considered, twelve EP values belong to each event. If the Event Probability is equal to zero (EP = 0), the corresponding permutation has a tagged b jet which is in the light jet position of the according permutation. As a consequence, if the number of Event Probabilities of all permutations which are equal to zero is zero, which means #(EP = 0) = 0, no tagged b jet is found in that event. But if #(EP = 0) = 6, only six permutations remain which indicates that one b jet is tagged. Finally, if #(EP = 0) = 10, there are just two permutations possible. As one has to differentiate between both the hadronic and the leptonic b jet, this result implies that two b jets are tagged in the event.
Thus, with the number of EP values which are equal to zero, the distinction between events with different numbers of tagged b jets is possible. The corresponding calculations are performed for all tested cut values. The results can be found in Table 6.4.

Additionally, there may occur events with more than two tagged b jets due to the

Cut value $W_{\text{cut}}^{\text{bjet}}$	No b-tag	One b-tag	Two b-tags	More b-tags
0	3450	7142	5855	19
1	3727	7546	5168	25
2	4031	7845	4566	24
3	4463	7928	4049	26
4	4947	7983	3514	22
5	5539	7933	2924	20
6	6108	7780	2557	21
7	6878	7384	2183	21
8	7628	7074	1743	21
9	8472	6586	1390	18
10	9367	5989	1096	14

Table 6.4: Number of events with no tagged b jets ("No b-tag"), one tagged b jet ("One b-tag"), two tagged b jets ("Two b-tags") and events with more tagged b jets for various cut values $W_{\text{cut}}^{\text{bjet}}$.

fact that all jets above a certain cut value are tagged as b jets. These events cannot be considered any longer and, consequently, the number of events used for a further analysis decreases. This comparatively small amount can also be seen in Table 6.4. In order to underline the difference between various cut values, the different numbers of tagged b jets are plotted in Fig. 6.4 for all tested cut values. The errors equal the square root of the number of events and are comparatively small. Hence, these errors are not visible in the plot.

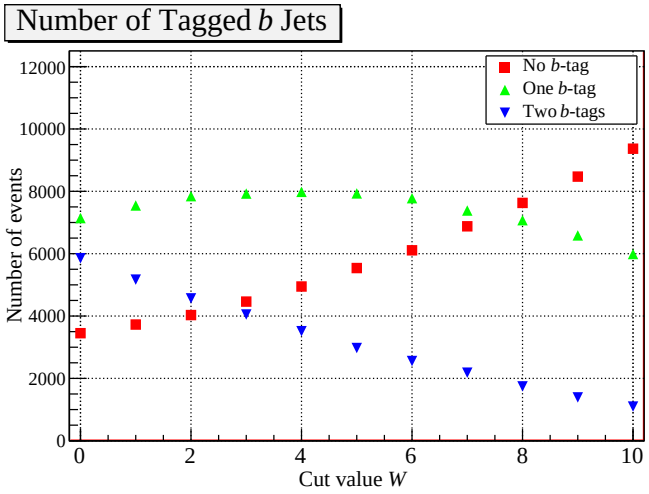

Figure 6.4: Number of events with no tagged b jets ("No b-tag"), one tagged b jet ("One b-tag") and events with two tagged b jets ("Two b-tags") for various cut values $W_{\text{cut}}^{\text{bjet}} \triangleq W$.

The fact that $W_{\text{cut}}^{\text{bjet}} = 2$ is the best cut value yielding high efficiencies leads to the conclusion that a large amount of events with one tagged b jet indicates appropriate and high efficiencies. Furthermore, approximately identical numbers of events with no and two identified b jets are required as it is revealed by the according Fig. 6.4. With larger cut values, the number of events with no tagged b jets increases while the number of events with two tagged b jets decreases. For cut values smaller than $W_{\text{cut}}^{\text{bjet}} = 2$, it is the other way round because more jets are tagged as b jets then, compliant with the shape of the jet weight distribution.

As mentioned in previous chapters, a proper top quark reconstruction supports the precise measurement of top quark properties like its mass. Since the KLFitter output file also contains an estimated top quark mass whose calculation is based on the reconstruction efficiency, these results can be examined at this point. For all different cut values used in the studies so far, the normalized top mass distributions are plotted. The results can be found in Fig. A.1 and A.2.

Three distributions for each cut value are plotted together, one includes the reconstructed top masses calculated from events with no tagged b jets, the other ones the masses originating from events with one or two tagged b jets, respectively. This differentiation was explored in depth in the previous paragraph. One can see a peak at about $m_t \approx 170 \ \frac{\text{GeV}}{c^2}$ which is close to the value 172.5 $\frac{\text{GeV}}{c^2}$, the sample generated top pole mass as mentioned in Chapter 5.2. Since the sample contains just a limited number of events, only slight differences between the plots and the three different distibutions in each figure are visible. However, on closer examination, it becomes obvious that the peak is more distinct in the case that both b jets are tagged properly. Furthermore, the distribution is more centered around the peak in this case. The same applies in the event that $W_{\text{cut}}^{\text{bjet}} = 2$ is used instead of another cut value leading to lower efficiencies.

Because of the quantity “Event Probability”, one can discriminate between events with no, with one or with two correctly identified b jets as it has just been done in order to determine the top mass distributions. Moreover, the different KLFitter efficiencies can be calculated separately for events with no tagged b jet, with one tagged b jet or with two tagged b jets. For these studies, the best cut value $W_{\text{cut}}^{\text{bjet}} = 2$ is chosen. The results are listed in Table 6.5 and confirm the presumptions based on the results of former studies. If only events are considered with no tagged b jets,

all efficiencies are comparatively low as the b-tagging efficiency does not reach large values. In the case that only events are taken into account with two b jets being tagged by the KLFitter, the b-tagging efficiency with $\varepsilon_b \approx 96\%$ is relatively high and consequently the probability of reconstructing the decay accurately is quite large, $\varepsilon_R \approx 79\%$, compared to the efficiencies one gets if all events are used.

Probability/ Efficiency	$W_{\text{cut}}^{\text{bjet}} = 2$ all events	$W_{\text{cut}}^{\text{bjet}} = 2$ no b-tag	$W_{\text{cut}}^{\text{bjet}} = 2$ one b-tag	$W_{\text{cut}}^{\text{bjet}} = 2$ two b-tags
P(all correct) [%]	65.14 ± 1.38	40.03 ± 2.62	63.27 ± 2.01	78.90 ± 2.49
$P(W_{\text{had}}$ correct) [%]	75.91 ± 1.49	46.91 ± 2.84	74.11 ± 2.17	91.37 ± 2.68
$P(b_{\text{had}}$ correct) [%]	68.70 ± 1.42	46.05 ± 2.81	67.03 ± 2.07	81.10 ± 2.52
$P(b_{\text{lep}}$ correct) [%]	77.69 ± 1.51	65.29 ± 3.35	78.57 ± 2.24	82.27 ± 2.54
P(b tag | truth b) [%]	87.47 ± 1.60	71.22 ± 3.50	86.83 ± 2.35	95.69 ± 2.74
P(b tag | light q) [%]	12.53 ± 0.60	28.78 ± 2.22	13.17 ± 0.92	4.31 ± 0.58
Number of Events	16466	4031	7845	4566

Table 6.5: Efficiencies of the KLFitter if only events with no tagged b jets ("no b-tag"), one tagged b jet ("one b-tag") or two tagged b jets ("two b-tags"), respectively, are considered. The cut value is $W_{\text{cut}}^{\text{bjet}} = 2$.

If only events with two correctly tagged b jets are considered, the number of events decreases as a lot of events are dismissed. Additionally, this leads to increasing statistical errors compared to the ones belonging to efficiencies which are calculated in the case that all selected events are used, which can be seen in Table 6.5. Therefore, another method which does not exclude certain events or permutations is considered.

6.3 b-Tagging by Using the Shape of the Jet Weight Distribution

In the last section a cut value was introduced in order to improve the reconstruction efficiency. Although this cut method was successful, further advance seems to be possible due to the fact that the likelihood function is set to zero if a b jet is regarded to be a light one which results in a loss of information. Moreover, this method implies a division of the jet weight distribution in just two parts. Since both jet weight distributions obtained from an *IP3DSV1* algorithm overlap (see Fig. 6.2), many light jets are tagged as b jets and vice versa. That is why there may occur events with more than two tagged b jets, which cannot be considered any longer,

leading to a decrease in the event selection efficiency. As mentioned in the last paragraph, this causes a larger error of the efficiencies.
For these reasons, a further b-tagging method is implemented utilizing the shape of both distributions. As the jet weight distributions provide the number of light jets, including charm jets, and the number of bottom jets, both having a certain weight, a probability whether a jet with this weight is a light or a b jet can be calculated. In this way, the shape of the distributions is used as the number of events belonging to a certain weight, making up this shape, are needed to evaluate this probability whereby N_b is the number of b jets having a jet weight W_{jet} and N_l is the number of light jets having this same jet weight.
If a certain jet with jet weight W_{jet} is regarded to be a jet originating from a b quark, the probability that the jet is a b jet is:

$$P_b = \frac{N_b}{N_b + N_l}.$$

If a certain jet with jet weight W_{jet} is regarded to be a light jet, the probability that the jet is a light jet is:

$$P_l = \frac{N_l}{N_b + N_l}.$$

$N_b + N_l$ is the number of all jets having the jet weight W_{jet}. A jet and the corresponding quark is regarded to be a light or a bottom one due to the theoretical quark position in the permutation for which the likelihood function L is calculated (see Equation (5.1)).
Instead of just multiplying this function by "1" or by "0", as it is done if the cut method is implemented, the likelihood function for each permutation is multiplied by the probability P_i $(i = b, l)$ with $0 \leq P_i \leq 1$ obtained from the number of jets having a certain weight. Accordingly, the likelihood function is weighted by the b-tagging information. Consequently, this method is also called "weight method".
Moreover, in order to improve the influence of the probability in the likelihood further, the logarithm of the probabilities P_b and P_l can be multiplied by an additional factor $f_s > 0$ before being added to the logarithm of the likelihood function. This factor enhances the b-tagging information relative to the kinematic fitting. Incidentally, the KLFitter uses the logarithm of the probability and furthermore of the whole likelihood function to accelerate the program and simplify its structure. The

KLFitter is tested with different scale factors f_s. The results of this method with scaled weights can be found in Table 6.6. The efficiencies from the original KLFitter version and the one using $W_{\text{cut}}^{\text{bjet}} = 2$ are also listed in order to facilitate a comparison between all different values.

Probability/Efficiency	No b-tag.	$W_{\text{cut}}^{\text{bjet}} = 2$	$f_s = 1$	$f_s = 2$
P(all correct) [%]	50.32 ± 1.21	65.14 ± 1.38	67.72 ± 1.41	69.35 ± 1.42
$P(W_{\text{had}}$ correct) [%]	57.86 ± 1.30	75.91 ± 1.49	78.78 ± 1.52	80.68 ± 1.54
$P(b_{\text{had}}$ correct) [%]	54.29 ± 1.26	68.70 ± 1.42	70.02 ± 1.43	71.54 ± 1.45
$P(b_{\text{lep}}$ correct) [%]	74.74 ± 1.48	77.69 ± 1.51	80.12 ± 1.53	80.36 ± 1.53
P(b tag | truth b) [%]	77.70 ± 1.51	87.47 ± 1.60	89.05 ± 1.61	90.05 ± 1.62
P(b tag | light q) [%]	22.30 ± 0.81	12.53 ± 0.60	10.95 ± 0.57	9.95 ± 0.54
Probability/Efficiency	$f_s = 3$	$f_s = 4$	$f_s = 5$	$f_s = 6$
P(all correct) [%]	69.52 ± 1.42	69.35 ± 1.42	69.30 ± 1.42	68.89 ± 1.42
$P(W_{\text{had}}$ correct) [%]	80.70 ± 1.54	80.40 ± 1.53	80.34 ± 1.53	79.81 ± 1.53
$P(b_{\text{had}}$ correct) [%]	71.94 ± 1.45	71.87 ± 1.45	71.95 ± 1.45	71.72 ± 1.45
$P(b_{\text{lep}}$ correct) [%]	80.38 ± 1.53	80.28 ± 1.53	80.16 ± 1.53	79.99 ± 1.53
P(b tag | truth b) [%]	90.03 ± 1.62	89.87 ± 1.62	89.85 ± 1.62	89.60 ± 1.62
P(b tag | light q) [%]	9.97 ± 0.54	10.13 ± 0.54	10.15 ± 0.54	10.40 ± 0.55
Probability/Efficiency	$f_s = 10$	$f_s = 30$	$f_s = 0.5$	$f_s = 0.75$
P(all correct) [%]	67.88 ± 1.41	66.42 ± 1.39	65.30 ± 1.38	66.59 ± 1.39
$P(W_{\text{had}}$ correct) [%]	78.93 ± 1.52	77.20 ± 1.50	75.91 ± 1.49	77.51 ± 1.50
$P(b_{\text{had}}$ correct) [%]	70.75 ± 1.44	69.56 ± 1.43	67.84 ± 1.41	69.04 ± 1.42
$P(b_{\text{lep}}$ correct) [%]	79.51 ± 1.52	78.51 ± 1.52	78.94 ± 1.52	79.76 ± 1.53
P(b tag | truth b) [%]	89.19 ± 1.61	88.35 ± 1.61	87.44 ± 1.60	88.36 ± 1.61
P(b tag | light q) [%]	10.81 ± 0.56	11.65 ± 0.58	12.56 ± 0.61	11.64 ± 0.58

Table 6.6: Efficiencies of the KLFitter for various scale factors f_s. Some results from former studies are also listed in order to compare the ones from both b-tagging methods.

The table reveals that without any additional scale factor, which conforms to $f_s = 1$, the reconstruction efficiency increases to about 68%. The results can be generalized to the statement that all efficiencies surpass the percentages from the KLFitter using b-tagging with cut values. Multiplying the logarithm of the probability by f_s leads to even higher efficiencies, depending on the chosen factor, only large factors, $f_s \gtrsim 30$, or small ones, $f_s \lesssim 0.5$, result in efficiencies lower than the ones from the cut method. The scale factor $f_s = 3$ leads to the highest efficiencies, the reconstruction efficiency reaches almost 70%, the b-tagging efficiency 90%. Scale factors $f_s < 1$

offer fast decreasing efficiencies.
Although this weight method leads to higher efficiencies, the errors of these values remain roughly in the same scale. They do not depend on the b-tagging method but on the number of events. This method uses more events than the previously presented cut method and thus a lower relative statistical error can be observed. Accordingly, the errors will also decrease if another sample containing more than 62,000 events is used.
In Fig. 6.5 the reconstruction and b-tagging efficiencies are plotted for several scale factors around the best one, $f_s = 3$.

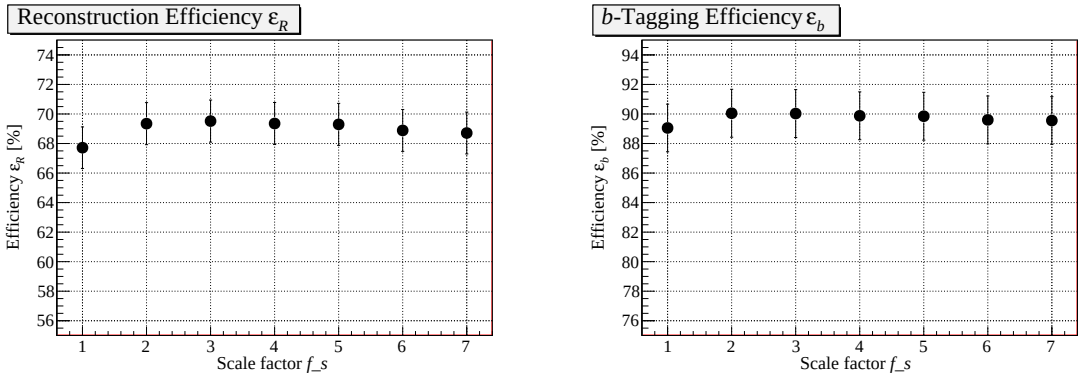

Figure 6.5: Reconstruction efficiencies (left) and b-tagging efficiencies (right) for various tested scale factors: $1 \leq f_s \leq 7$.

Both efficiencies decrease if $f_s > 3$, but all plotted values exceed the ones originating from the first b-tagging cut method. The efficiency plots for each scale factor including all efficiencies can be found in Fig. A.5 and A.6 in order to visualize the differences between various utilized scale factors.
The use of an additional scale factor can improve the efficiencies further because in this case the b-tagging information is given more or less weight, depending on the factor. Therefore, with this scale factor, the difference between the original (kinematic fitting) part of the likelihood function and the additional part containing the b-tagging information is altered. A large scale factor gives more weight to the b-tagging part than to the kinematic fitting part, a small one causes an underestimation of the weight of the b-tagging information.
Incidentally, the extreme cases of the scale factor can be discussed. In the case that small scale factors ($f_s \to 0$) are used, the efficiencies decrease further. $f_s = 0$ corresponds to the KLFitter version with no implemented b-tagging so that $\varepsilon_R \approx 50\%$

and $\varepsilon_b \approx 78\%$ in accordance with Table 6.3 are expected. A KLFitter version with large scale factors ($f_s \to \infty$) equals the one which just depends on b-tagging not using any kinematic fitting. In this case, with larger scale factors, the efficiencies approach the values $\varepsilon_R \approx 32\%$ and $\varepsilon_b \approx 81\%$, respectively, as shown in Table 6.3. $f_s = 3$ can be regarded as an appropriate and empirically determined middle course.

6.4 Comparison of the Different Methods

Two different b-tagging methods implemented in the KLFitter were analyzed in the last sections. Both were compared with the original version of this tool for kinematic fitting where b-tagging information is not used for the fit. This reveals that, as it was theoretically predicted, the probability of identifying b jets, the b-tagging efficiency, increases in the case that b-tagging methods are used. Therefore, the reconstruction efficiency of the whole decay increases as well. A further comparison between both b-tagging methods shows that the weight method leads to even higher efficiencies than the first one yield due to the fact that, if the second one is implemented, the shape of the jet weight distribution serves for the identification of jets and that not only a cut value divides the distribution in simply two parts.

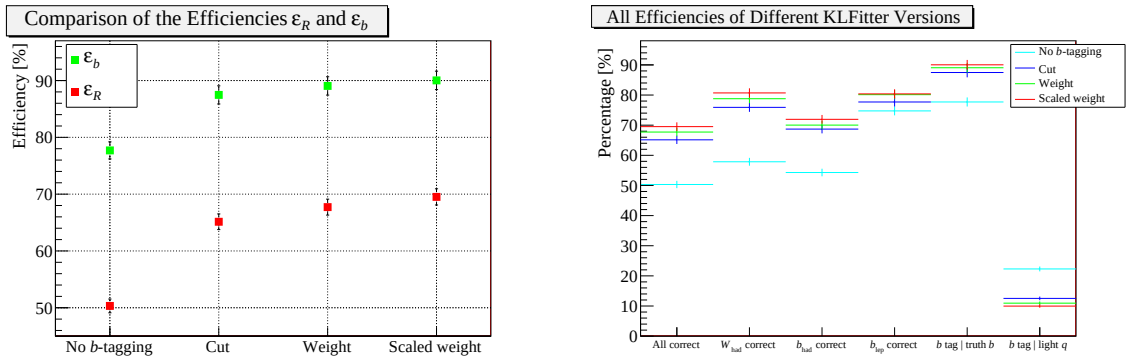

Figure 6.6: ε_b and ε_R of different versions of the KLFitter (left) and all efficiencies of these versions (right); original version ("No b-tagging"), KLFitter with implemented b-tagging based on cut values $W_{\text{cut}}^{\text{bjet}} = 2$ ("Cut") or based on the shape of the jet weight distribution with $f_s = 1$ ("Weight") and $f_s = 3$ ("Scaled weight").

Accordingly, the b-tagging efficiency ε_b reaches 89% instead of 87% ("best" cut value $W_{\text{cut}}^{\text{bjet}} = 2$), the reconstruction efficiency ε_R is about 68%, compared with 65%. However, independent of the used method, both ones constitute a considerable

improvement which becomes obvious by regarding the efficiencies of the original version of the KLFitter with $\varepsilon_b \approx 78\%$ and $\varepsilon_R \approx 50\%$. Moreover, an additional scale factor f_s multiplied with the probability $\log(P_i)$, calculated in the case that the weight method is employed, causes a further increase in the efficiencies: $\varepsilon_b \approx 90\%$ and $\varepsilon_R \approx 70\%$. These values can be found in the left plot of Fig. 6.6 showing the incremental increase in these two efficiencies if more sophisticated b-tagging methods are implemented. All efficiencies of these KLFitter versions can be seen in the right plot in order to illustrate the difference between all of them.
A correct top quark reconstruction supports the precise measurement of top quark properties like its mass, as described in Section 6.2, being the reason for all attempts to improve the reconstruction efficiency. With the KLFitter output file containing an estimated top quark mass based on the reconstruction efficiency, the results of the top quark mass calculation can be examined for the different b-tagging algorithms.

The mass distributions for all four different versions of the KLFitter, whose efficiencies are plotted in Fig. 6.6, seem to be most interesting for further analysis. The shape of the distributions resemble those presented in Section 6.2. A peak occurs at about $m_t \approx 170\ \frac{\text{GeV}}{c^2}$, close to the true value $M_{\text{top}} \approx 172.5\ \frac{\text{GeV}}{c^2}$. The distributions are not plotted explicitly because only slight differences between these distributions are visible due to the limited number of events in the sample.
In order to describe the shape mathematically, a Gaussian curve is fitted to the top mass distribution around the peak. As the curve is only fitted to the peak of the distribution, a Gaussian curve instead of a Breit-Wigner one is used. It is expected that the Gaussian curve has a smaller width with a more distinctive peak if the distribution originating from the KLFitter with cut value $W_{\text{cut}}^{\text{bjet}} = 2$ is used in comparison to the original fitter version. Consequently, considering also the top mass calculations in Chapter 6.2, one can actually deduce that a higher reconstruction efficiency of top quark decays caused by the implementation of b-tagging methods in the KLFitter results in a more precise measurement of the top quark properties as its mass due to the more distinctive peak. The top mass distribution for the KLFitter with the b-tagging method using the scale factor $f_s = 3$ do not significantly improve the shape of the top mass distribution further, but the number of events increases which is also very important for a precise top mass measurement.
Summarized, the result is a reduction of combinatorical background from the fitting procedure. b-tagging also improves the background rejection in order to have a high purity sample in data.

In this thesis, as this section revealed, evermore sophisticated b-tagging methods have been presented. As the methods get more and more complex, more different uncertainties have to be considered. The errors of the KLFitter version which does not use any b-tagging information only depend on statistical uncertainties. If the cut method is implemented, one also has to regard the error of chosing an adequate cut value. Therefore, different tests with various cut values are essential. The weight method utilizes the shape of the distribution. Consequently, the errors of all entries in the corresponding plot has to be taken into account. Especially at the borders of the distribution with only a limited number of jets having a certain weight, the uncertainties of the b-tagging information are quite large. Furthermore, the use of an additional scale factor requires an adequate knowledge of the influence of this factor on the efficiencies. Hence, more and more sophisticated b-tagging methods lead to an increasing number of sources of error.

6.5 Calculation of the Total Efficiency

In the studies presented in the previous sections, the main goal was an enhancement of the reconstruction efficiency ε_R of top quark decays by implementing several b-tagging methods in the KLFitter. Thus, the b-tagging efficiency ε_b and ε_R were the most important quantities for the analysis. But ε_R is not equivalent to the total efficiency of the KLFitter because the calculation of the reconstruction efficiency is based on all events passing the selection criteria. However, not all of these events fulfill the matching criterion, mentioned in Chapter 5.2. Hence, the *total efficiency* ε_{tot} of the KLFitter is smaller than ε_R. By evaluating an additional *matching efficiency* ε_M, this fact can be taken into account. The matching efficiency is defined as the ratio of all events fulfilling the matching criteria N_M and all selected events N_S: $\varepsilon_M = \frac{N_M}{N_S}$. The total efficiency can then be calculated according to:

$$\varepsilon_{\text{tot}} = \varepsilon_M \cdot \varepsilon_R. \tag{6.2}$$

This total efficiency will be used for further studies. Pursuant to the event selection criteria presented in Chapter 5.2, there are four jets needed, having a transverse momentum p_T larger than 20 $\frac{\text{GeV}}{c}$. For the studies so far, all events with four or more jets fulfilling this criterion were taken into consideration. The four jets with highest

p_T were then used for the fit. Although just semileptonic top quark pair decays are regarded, there may occur events with more jets due to higher order corrections.
It can be implemented in the KLFitter that only events with exactly four, five or six jets having such a transverse momentum are considered. Furthermore, the KLFitter allows for different numbers of jets used for fitting so that the KLFitter can fit either four, five or even six jets.
The studies testing the performance of the KLFitter have been done with the old version of this program, not employing any additional b-tagging method. The numbers are obtained from a sample with $\sqrt{s} = 10$ TeV. The results of these tests can be found in Table 6.7 [33], explicit information about the errors is not available.

Number of jets in event	Number of jets used for fitting	ε_M [%]	ε_R [%]	ε_{tot} [%]
4	4	36.62	54.31	19.98
5	4	14.99	52.46	7.86
	5	49.26	27.81	13.67
6	4	7.41	49.88	3.56
	5	28.15	29.34	8.26
	6	53.94	14.94	8.06
4/5/6	4/4/4	24.02	59.91	12.94
4/5/6	4/5/5	39.86	39.55	15.76

Table 6.7: For a certain number of jets the matching, the reconstruction as well as the total efficiencies are calculated for the possible number of fitted jets. In the last two rows two feasible setups of the original KLFitter version are presented. In the first, the four jets with highest p_T are used for the fit, in the second, five jets are used for jet multiplicities exceeding four. The numbers are obtained from a sample with $\sqrt{s} = 10$ TeV [33].

In the framework of this thesis, these studies can be redone with a modified version of the KLFitter which calculates the reconstruction efficiency with the help of b-tagging information. Again, the sample used for all analyses previously presented with $\sqrt{s} = 7$ TeV is utilized. The results presented in the last Chapter 6.4 show that the b-tagging method using the shape of the jet weight distribution with $f_s = 3$ leads to the highest reconstruction efficiency. Performing the studies with this KLFitter version results in the efficiencies that can be seen in Table 6.8.
As both tables reveal, events containing four, five or six jets are selected. Either four, five or six jets are then used for fitting depending on the number of jets in the event which has to exceed the number of jets in the fit. It becomes obvious that,

Num. of jets in event	Num. of jets used for fitt.	ε_M [%]	ε_R [%]	ε_{tot} [%]
4	4	44.22 ± 0.67	68.96 ± 1.70	30.49 ± 0.88
5	4	19.16 ± 0.60	70.20 ± 3.00	13.45 ± 0.71
	5	54.76 ± 0.76	28.97 ± 1.14	15.86 ± 0.66
6	4	9.90 ± 0.66	70.56 ± 5.98	6.99 ± 0.75
	5	31.27 ± 1.03	33.22 ± 2.33	10.39 ± 0.80
	6	54.48 ± 1.11	12.87 ± 1.11	7.01 ± 0.62
4/5/6	4/4/4	29.36 ± 0.42	69.34 ± 1.43	20.36 ± 0.51
4/5/6	4/5/5	45.79 ± 0.46	48.50 ± 1.02	22.21 ± 0.52

Table 6.8: The same numbers as presented in Table 6.7, but now the KLFitter is based on the weight method with scale factor $f_s = 3$. The numbers are obtained from the sample used for all other studies previously presented with $\sqrt{s} = 7$ TeV.

in case that four jets are used for fitting, ε_R is quite large. This efficiency decreases if more jets are considered. But as the matching efficiency ε_M increases with the number of jets in the fit, ε_{tot} increases with this number. Thus, utilizing more than four jets leads to an improvement of the total efficiency although being considerably smaller than ε_R.

In the last two rows of the tables, two possible setups of the KLFitter are presented. In each case, events with four, five or six jets are taken into account. In the first setup, always the four highest jets in p_T are used for fitting and, in the second, five jets are used if the jet multiplicity exceeds four resulting in a higher ε_{tot}.

A comparison between the efficiencies of both KLFitter versions clearly shows that the one based on an additional b-tagging method leads to higher total efficiencies ε_{tot} as this efficiency depends on both ε_R and ε_M (see Equation (6.2)). The increase in ε_M, which can be seen by a comparison between Table 6.7 and Table 6.8, is due to the fact that the samples were generated at different center-of-mass energies. A higher center-of-mass energy causes more boosts resulting in a lower matching efficiency. The increase in ε_R has already been analyzed in former chapters. The total efficiency reaches for both setups about 20% and 22%. The original version of the KLFitter just allows for about 13% and 16%, respectively, at a higher center-of-mass energy.

The error of ε_R, indicated in Table 6.8, is calculated by the Top Histogram Maker on the basis of the KLFitter output file. The one of ε_M corresponds to the error originating from a binomial distribution. Finally, as ε_{tot} depends on both ε_R and ε_M, according to Equation (6.2), the error of the total efficiency results from the

ones of ε_R and ε_M by means of error propagation.

7 Conclusion

In this bachelor's thesis, the impact of several b-tagging algorithms on the reconstruction of top-antitop quark pairs decaying semileptonically into four jets and one electron have been analyzed by use of the KLFitter, a tool for kinematic fitting based on a likelihood approach. The main goal has been to improve the reconstruction efficiency ε_R of the KLFitter in order to enhance the measurement of top quark properties like the top mass based on an adequate reconstruction of the decay of this heaviest quark.

At first, the initial version of the KLFitter not depending on any b-tagging information was tested. In this case, the calculation of efficiencies was only based on kinematic fitting. The b-tagging efficiency ε_b reached 78%, the reconstruction efficiency at least 50%. Compared to the values derived from pure statistics, these efficiencies were quite appropriate but special b-tagging methods should improve ε_b further and thus ε_R as well.
Both analyzed algorithms used the jet weight distribution, calculated by an *IP3DSV1* tagger. The first b-tagging method implemented in the KLFitter was based on a certain cut value of the jet weight. All jets having a jet weight exceeding this value were tagged as b jets while jets having a weight below this cut value were identified as light jets. The studies revealed that the cut value $W_{\mathrm{cut}}^{\mathrm{bjet}} = 2$ led to the highest efficiencies with $\varepsilon_b \approx 87\%$ and $\varepsilon_R \approx 65\%$. Furthermore, this improvement caused a narrowing of the top mass distribution with a more distinctive peak, especially if just events with two correctly tagged b-jets are considered.
Subsequently, the second b-tagging method was tested, utilizing the shape of the jet weight distribution. A probability whether a jet is a light or a b jet could be derived from this shape and was then added to the likelihood function. By multiplying the logarithm of this function with a scale factor f_s, the b-tagging information could be weigthed compared to the kinematic information. The highest efficiencies were achieved with a scale factor $f_s = 3$. ε_b increased to 90%, ε_R reached about 70%,

underlining that this method surpassed the first.
As not all events used for the calculation of ε_R fulfilled a certain matching criterion, an additional matching efficiency ε_M had to be taken into account in order to evaluate the total efficiency ε_{tot} of the KLFitter. This was done in a supplementary analysis. When a convenient setup of the KLFitter was used, ε_{tot} reached 22% compared to 16% obtained from older studies with the original KLFitter version at a higher center-of-mass energy.

Consequently, it can be determined that b-tagging information added to the KLFitter improves the b-tagging efficiency and in this context the reconstruction efficiency as well, being essential for a more precise measurement of the top quark properties. With the improvements of the KLFitter, established in the framework of this thesis, it has become a promising tool for analyzing top quark decays being detected by the ATLAS detector at the LHC in the near future, thus helping to measure the properties of the heaviest quark as its mass.

A Additional Plots

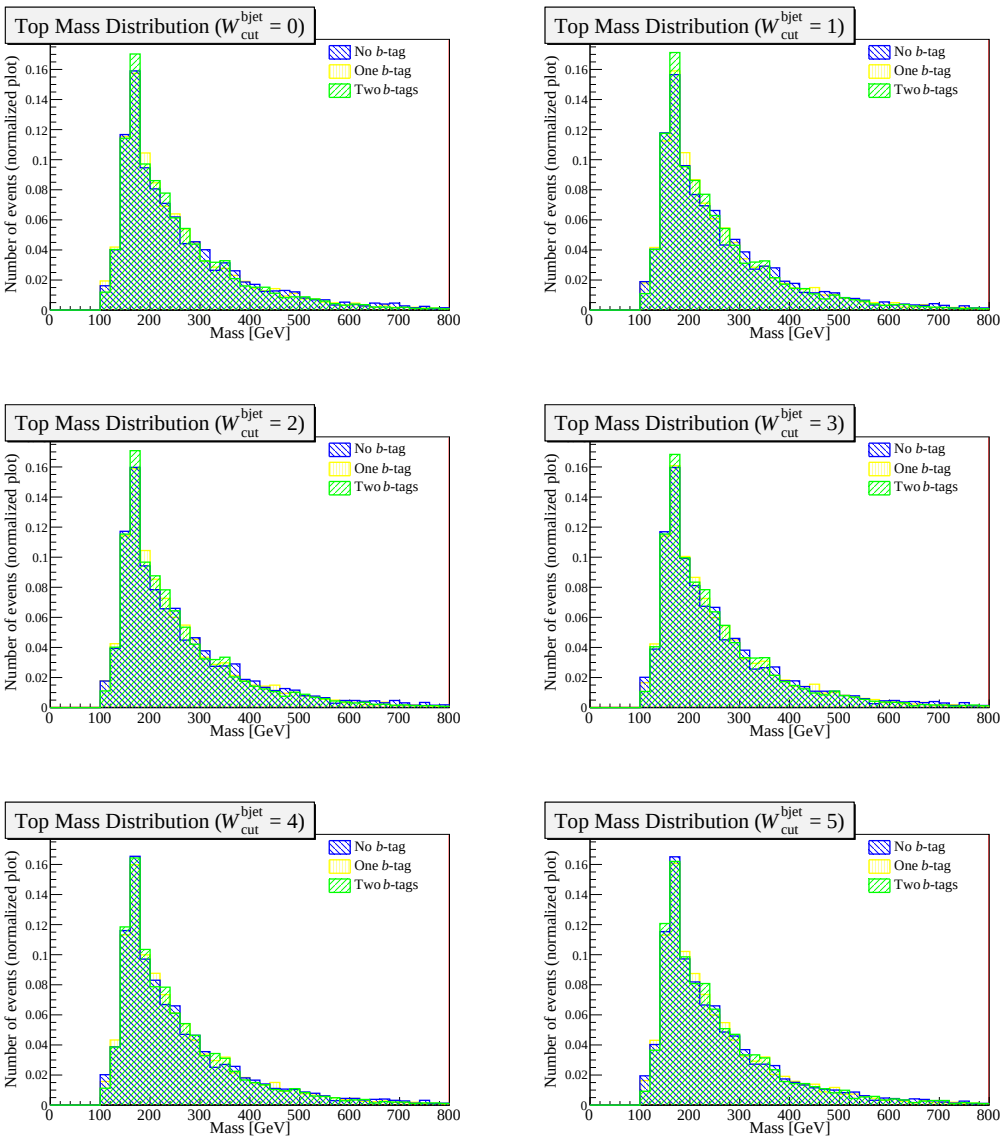

Figure A.1: Top mass distributions for events with no tagged b jets ("No b-tag"), one tagged b jet ("One b-tag") and events with two tagged b jets ("Two b-tags") in the case that cut values $W_{\text{cut}}^{\text{bjet}}$ in the range between 0 and 5 are used.

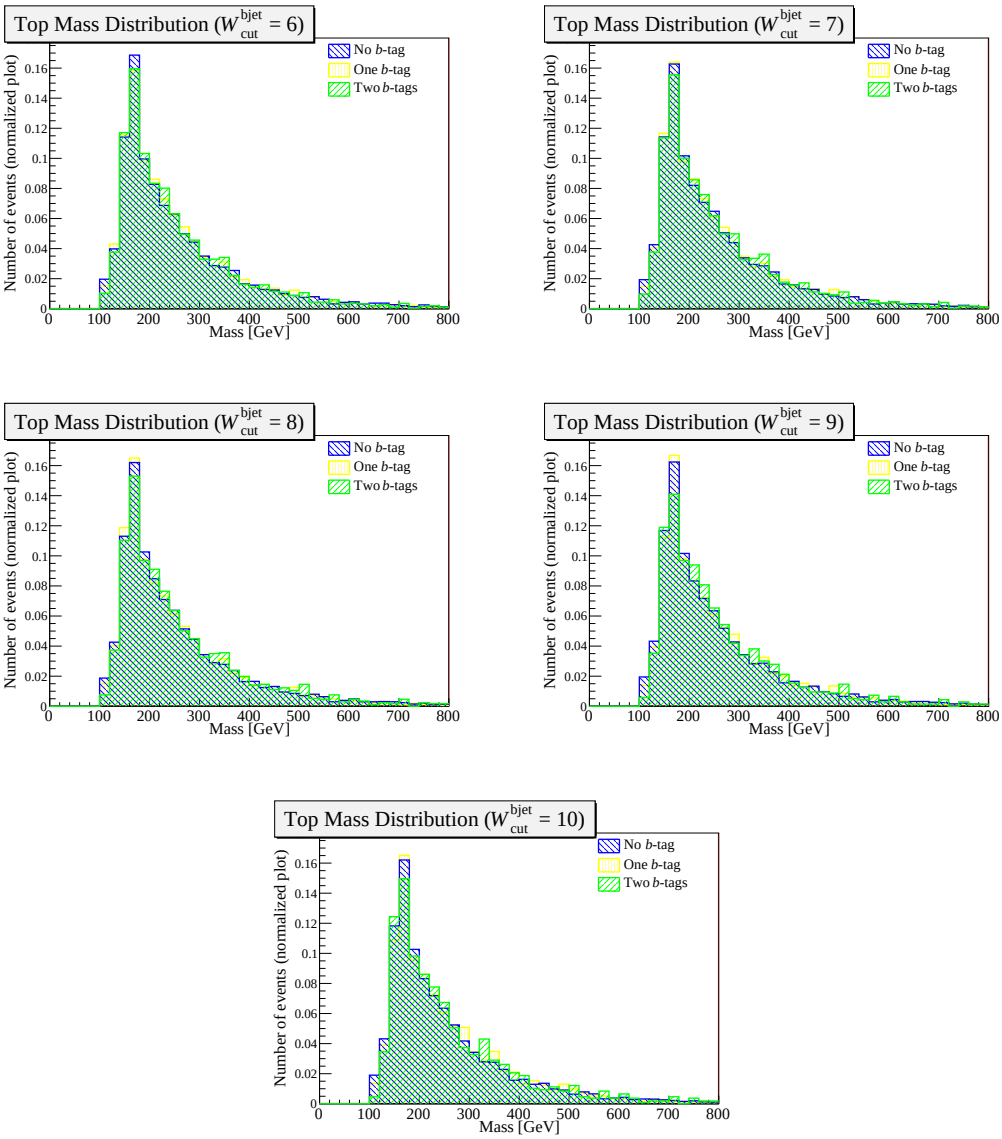

Figure A.2: Top mass distributions for events with no tagged b jets ("No b-tag"), one tagged b jet ("One b-tag") and events with two tagged b jets ("Two b-tags") in the case that cut values $W_{\text{cut}}^{\text{bjet}}$ in the range between 6 and 10 are used.

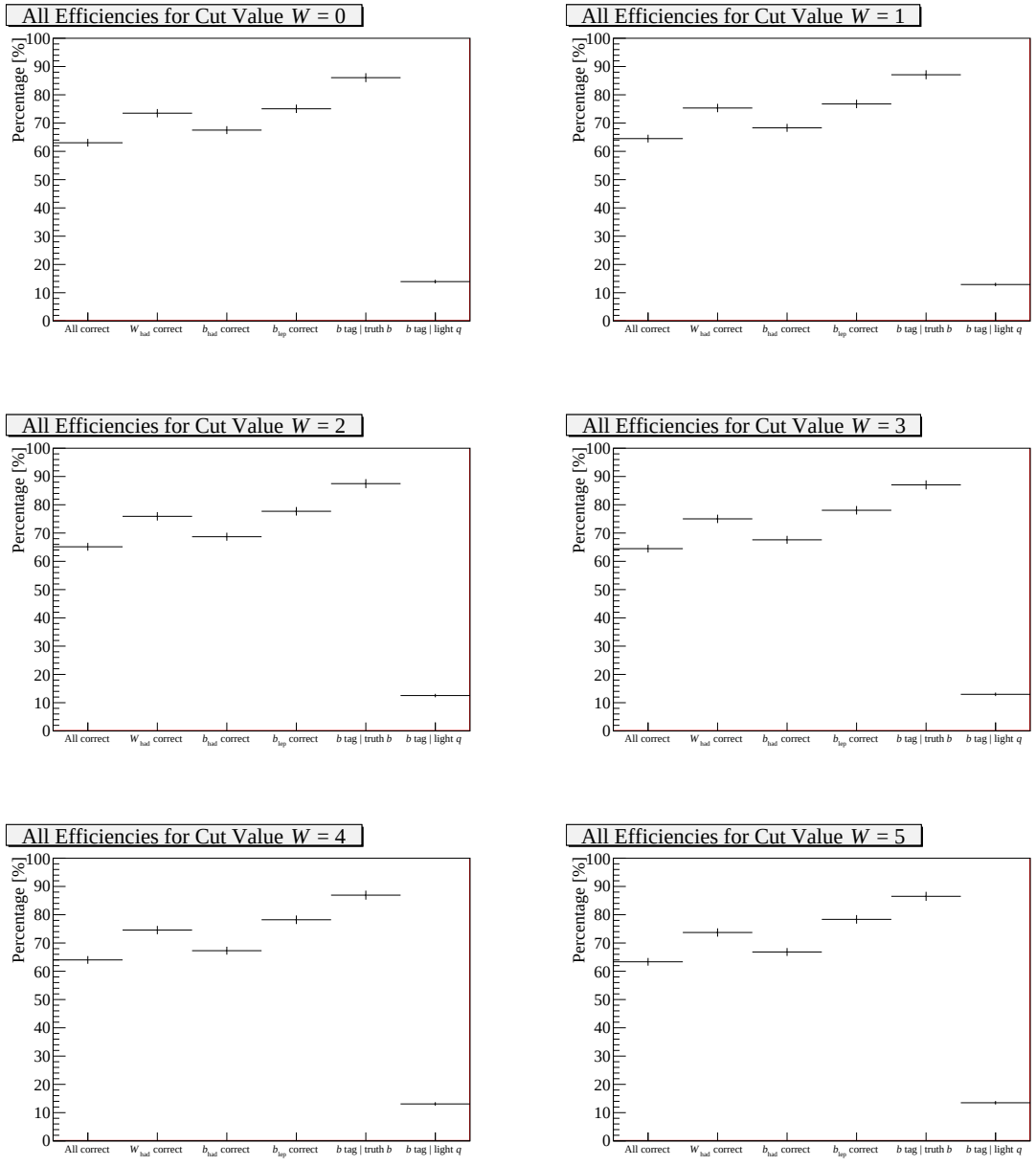

Figure A.3: Plots showing the efficiencies of the KLFitter for various cut values $W_{\text{cut}}^{\text{bjet}} \triangleq W$ in the case that the corresponding b-tagging method with cut values is used (first six plots).

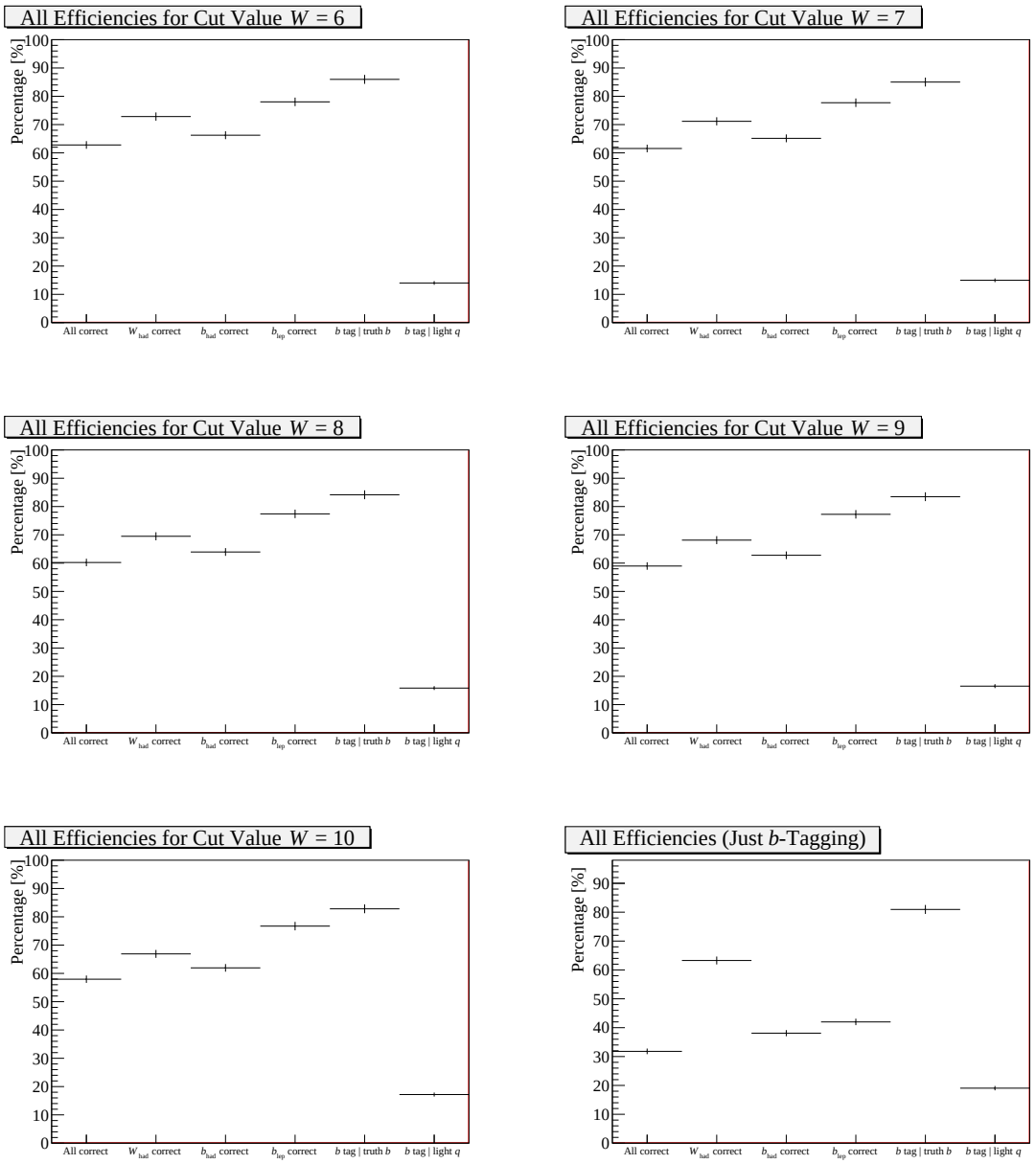

Figure A.4: Plots showing the efficiencies of the KLFitter for various cut values $W_{\text{cut}}^{\text{bjet}} \triangleq W$ in the case that the corresponding b-tagging method with cut values is used (last five plots). The plot on the bottom right shows the efficiencies if the KLFitter version just depending on the b-tagging information, without kinematic fitting, is used.

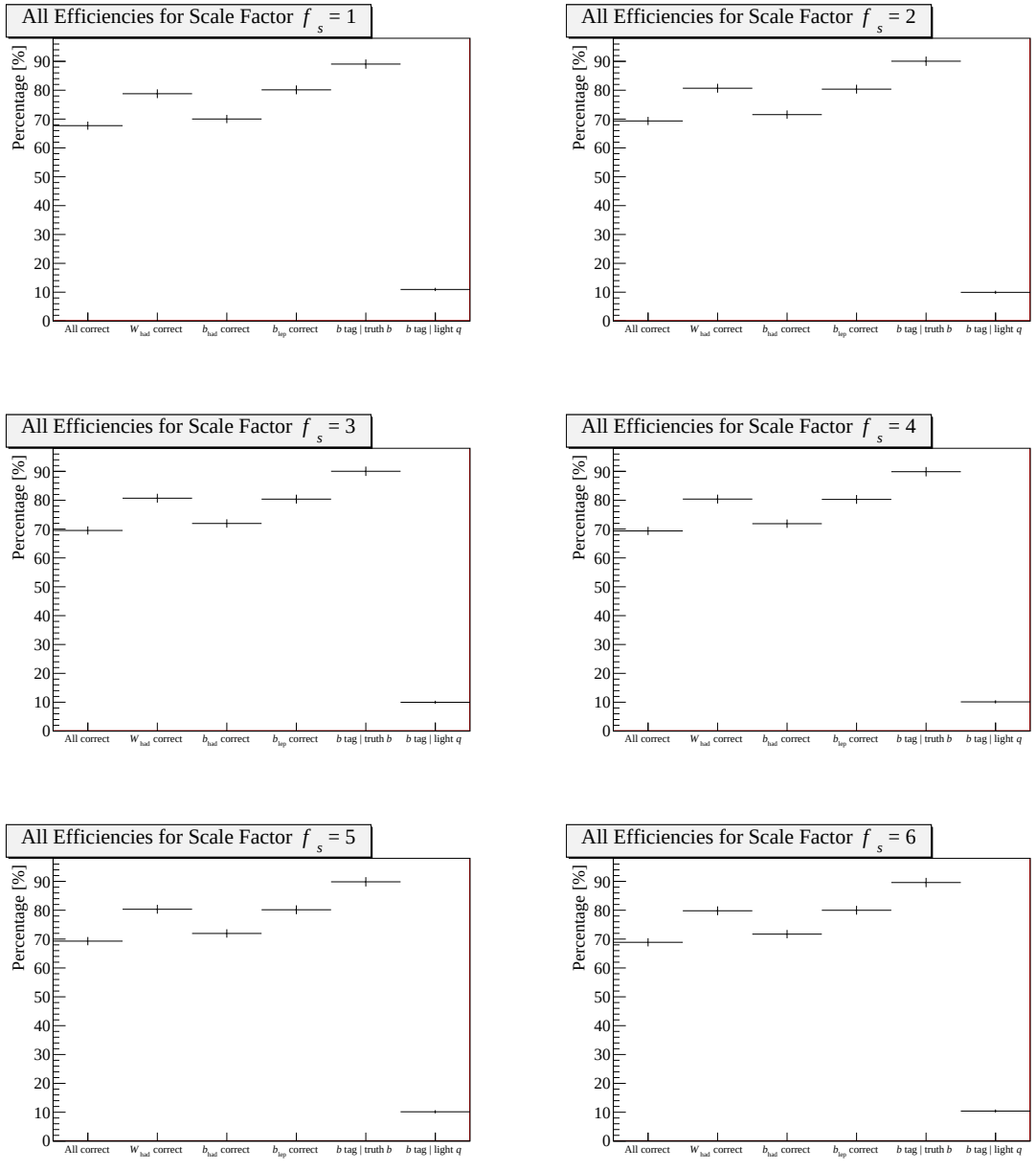

Figure A.5: Plots showing the efficiencies of the KLFitter for various scale factors f_s in the case that the corresponding b-tagging method depending on the shape of the jet weight distribution is used (first six plots).

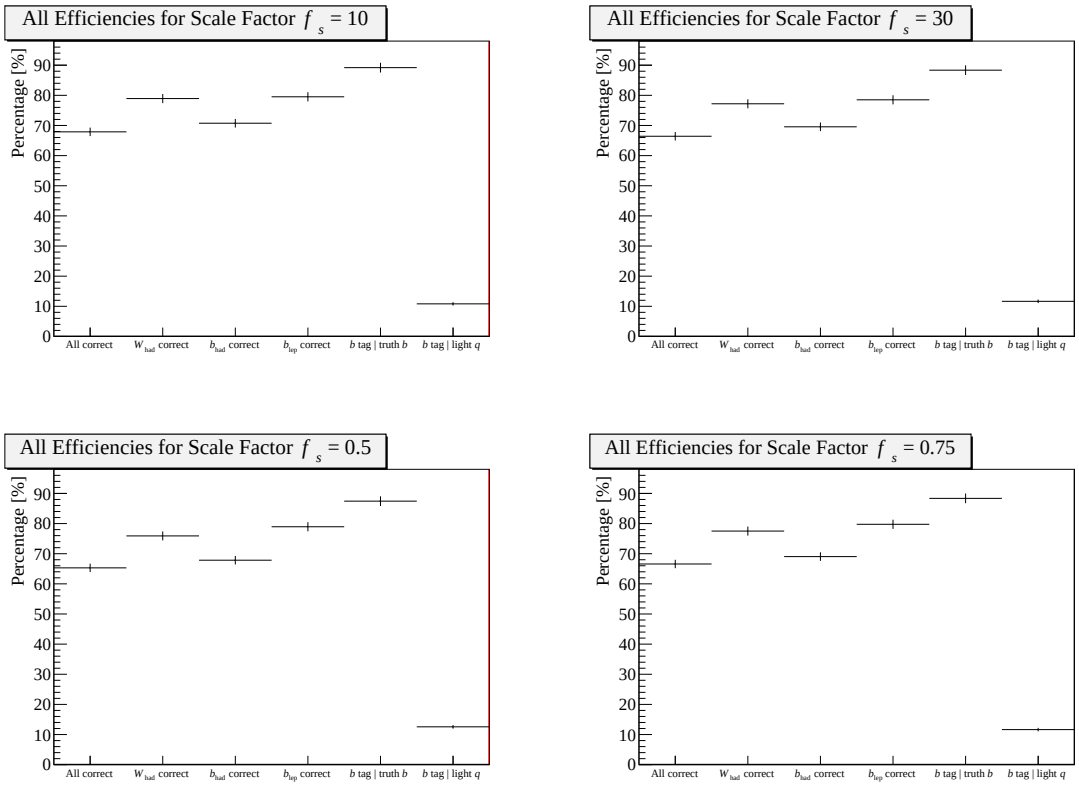

Figure A.6: Plots showing the efficiencies of the KLFitter for various scale factors f_s in the case that the corresponding b-tagging method depending on the shape of the jet weight distribution is used (last four plots).

Nomenclature

Variables

Variable	Meaning
$\mathcal{B}$	branching ratio
C	colour
CP	charge parity
CPT	charge parity time
E and E_T	energy and transverse energy
f_s	scale factor
m or M	mass
N_c	color factor
p and p_T	momentum and transverse momentum
P	probability
Q	electric charge
R_l	rejection
ΔR	distances in the η-ϕ-plane
s	spin
$\sqrt{s}$	center-of-mass energy
T	weak isospin
T_3	weak isospin (third component)
V	CKM matrix
W	jet weight
$W_{\text{cut}}^{\text{bjet}}$	cut value
x	Bjorken-x
Y	hypercharge
α_s	QCD coupling
η	pseudorapidity
λ_k	Gell-Mann matrices ($k = 1, ..., 8$)

Variable	Meaning
Γ	decay width
Ω	direction
ϕ	azimuthal angle
σ	cross section
σ_i	Pauli matrices ($i = 1, 2, 3$)
τ	lifetime
θ	polar angle

Efficiencies

Efficiency	Meaning
ε_b	b-tagging efficiency
ε_M	matching efficiency
ε_R	reconstruction efficiency
ε_{tot}	total efficiency

Particles

Particle	Meaning
b	bottom quark
c	charm quark
d	down quark
e	electron
g	gluon
$p/\bar{p}$	proton/antiproton
$q/\bar{q}$	quark/antiquark
s	strange quark
t	top quark
u	up quark
W	W boson
Z	Z boson
γ	photon

Particle	**Meaning**
μ	muon
ν	neutrino
τ	tau

Abbreviations

Abbreviation	**Meaning**
ATLAS	A Toroidal LHC Apparatus
BW	Breit-Wigner
CKM	Cabibbo-Kobayashi-Maskawa (matrix)
EP	Event Probability
G_F	Fermi coupling constant
IP	impact parameter
KLFitter	Kinematic Likelihood Fitter
L	likelihood function
LHC	Large Hadron Collider
MC	Monte Carlo
PDG	Particle Data Group
SM	Standard Model of Elementary Particle Physics
SU	special unitary group
SV	secondary vertex
U	unitary group
W	transfer function
θ_W	Weinberg angle

List of Figures

List of Tables

Bibliography

[1] C. Amsler et al. (Particle Data Group), Review of Particle Physics, *Phys. Lett.*, B667, 1 (2008) and 2009 partial update for the 2010 edition, 2009.

[2] D. Griffiths, *Introduction to Elementary Particles*, WILEY-VCH, 2nd edition, 2008.

[3] B. Povh, K. Rith, C. Scholz, and F. Zetsche, *Teilchen und Kerne: Eine Einführung in die physikalischen Konzepte*, Springer, 8th edition, 2009.

[4] C. Berger, *Elementarteilchenphysik: Von den Grundlagen zu den modernen Experimenten*, Springer, 2nd edition, 2006.

[5] F. Halzen and A. D. Martin, *Quarks and Leptons: An Introductory Course in Modern Particle Physics*, John Wiley and Sons, 1984.

[6] P. W. Higgs, Broken Symmetries and the Masses of Gauge Bosons, *Phys. Rev. Lett.*, 13:508–509, 1964.

[7] The CDF Collaboration, T. Aaltonen et al., Observation of Top Quark Production in $\bar{p}p$ Collisions, *Phys. Rev. Lett.*, 74:2626–2631, 1995.

[8] The DØ Collaboration, S. Abachi et al., Observation of the Top Quark, *Phys. Rev. Lett.*, 74:2632–2637, 1995.

[9] The DØ Collaboration, V. M. Abazov et al., Observation of single top-quark production, *Phys. Rev. Lett.*, 103:092001, 2009.

[10] The CDF Collaboration, T. Aaltonen et al., First Observation of Electroweak Single Top Quark Production, *Phys. Rev. Lett.*, 103:092002, 2009.

[11] The Tevatron Electroweak Working Group for the CDF and DØ Collaborations, Combinations of CDF and DØ Results on the Mass of the Top Quark, *arXiv:1007.3178v1 [hep-ex]*, 2010.

[12] M. Jezabek and J. H. Kühn, QCD corrections to semileptonic decays of heavy quarks, *Nucl. Phys.*, B 314, 1 (1989), 1989.

[13] A. Czarnecki and K. Melnikov, Two-loop QCD corrections to top quark width, *Nucl. Phys.*, B 554 (1999) 520, 1999.

[14] K. G. Chetyrkin et al., Second Order QCD Corrections to $\Gamma(t \to Wb)$, *Phys. Rev.*, D 60 (1999) 114015, 1999.

[15] J. Pumplin et al., New Generation of Parton Distributions with Uncertainties from Global QCD Analysis, *JHEP*, 0207:012, 2002.

[16] A. Quadt, Top quark physics at hadron colliders, *Eur. Phys. J. C*, 48:835–1000, 2006.

[17] C. Clément, Tevatron Top Results, *arXiv:hep-ex/0605111v1*, 2006.

[18] W. Bernreuther, Top quark physics at the LHC, *arXiv:0805.1333v1 [hep-ph]*, 2008.

[19] O. Brüning, P. Collier, P. Lebrun, S. Myers, R. Ostojic, J. Poole and P. Proudlock, *LHC Design Report: Volume I The LHC Main Ring*, CERN, 2004.

[20] The ALICE Collaboration, *ALICE: Technical Design Report of the Transition Radiation Detector*, CERN, 2001.

[21] LHCb: Technical Proposal, *CERN-LHCC-98-004*, 1998.

[22] The CMS Collaboration, G. L. Bayatian et al., CMS physics: Technical Design Report, *CERN-LHCC-2006-001*, 2006.

[23] The ATLAS Collaboration, G. Aad et al., The ATLAS Experiment at the CERN Large Hadron Collider, *JINST*, 3:S08003, 2008.

[24] M. Lehmacher, b-Tagging Algorithms and their Performance at ATLAS, *arXiv:0809.4896v3 [hep-ex]*, 2008.

[25] K. Hanagaki, b-tagging at DØ, *fermilab-conf-05-647-e*, 2005.

[26] The ROOT Team, *ROOT: User's Guide 5.26*, CERN, 2009.

[27] A. Caldwell, D. Kollar and K. Kröninger, BAT - The Bayesian Analysis Toolkit, *Comput. Phys. Commun.*, 180 (2009) 2197, 2009.

[28] S. Frixione and B.R. Webber, Matching NLO QCD Computations and Parton Shower Simulations, *JHEP*, 0206 (2002) 029, 2002.

[29] S. Frixione, P. Nason and B.R. Webber, Matching NLO QCD and Parton Showers in Heavy Flavour Production, *JHEP*, 0308 (2003) 007, 2003.

[30] P. Calafiura et al., The Athena Control Framework in Production, New Developments and Lessons Learned, In *Computing in High Energy Physics and Nuclear Physics 2004*, pages 456–458. CERN, 2005.

[31] G. Soyez, The SISCone and anti-k_t jet algorithms, *arXiv:0807.0021v1 [hep-ph]*, 2008.

[32] The ATLAS Collaboration, G. Aad et al., Expected Performance of the ATLAS Experiment: Detector, Trigger and Physics, *arXiv:0901.0512v4 [hep-ex]*, 2009.

[33] O. Nackenhorst, Top Quark Pair Reconstruction in the Electron + Jets Channel with a Kinematic Likelihood Fitter in the ATLAS Experiment, *Diploma Thesis*, II.Physik-UniGö-Dipl-2010/04, Göttingen, 2010.

Acknowledgements

In the first instance, I would like to thank Prof. Dr. Arnulf Quadt for offering me the opportunity to write my bachelor's thesis in his department and for being the first referee. I am also very thankful to Prof. Dr. Ariane Frey for her readiness to be the second referee. In this context, I wish to express my gratitude to the two of them for their instructive, interesting and sometimes even exciting and entertaining lectures. Their contagious enthusiasm for particle physics encouraged me to write my bachelor's thesis in this field of physics.

I am much obliged to Stefan Guindon for supervising my work so dedicated and especially for answering all my questions concerning top quark physics or programming. I am very grateful for his patience in solving problems with my computer, for proof-reading and, of course, for answering my questions about the English language.
Sincere thanks to Dr. Kevin Kröninger for supervising my bachelor's thesis as well, for discussing all achieved results, for answering all organizational questions and, last but not least, for proof-reading.
I would also like to thank Johannes Erdmann, Olaf Nackenhorst and Sven Ebert for solving all problems which emerged related to the KLFitter.

Furthermore, I am very grateful to two of my former teachers at school, Peter Fellenberg and Kirstin Oberdorf, who arouse my enthusiasm for physics due to their always informative and fascinating lessons.
Special thanks to my parents for their mental support during the last years, especially during the last few months, while I was working on this thesis.

Erklärung nach §13(8) der Prüfungsordnung für den Bachelor-Studiengang Physik und den Master-Studiengang Physik an der Universität Göttingen:

Hiermit erkläre ich, dass ich diese Abschlussarbeit selbständig verfasst habe, keine anderen als die angegebenen Quellen und Hilfsmittel benutzt habe und alle Stellen, die wörtlich oder sinngemäß aus veröffentlichten Schriften entnommen wurden, als solche kenntlich gemacht habe.
Darüberhinaus erkläre ich, dass diese Abschlussarbeit nicht, auch nicht auszugsweise, im Rahmen einer nichtbestandenen Prüfung an dieser oder einer anderen Hochschule eingereicht wurde.

Göttingen, den 19. Juli 2010

(Philipp Stolte)